

An assessment of the potential for cloud computing and satellite thermal infrared sensing to produce meaningful river temperature insights for hydropower operations

Samuel James Valman

Supervised by: Dr Stephen Dugdale and Professor Doreen Boyd

Nottingham Geospatial Institute, Nottingham, UK

Dissertation submitted to The University of Nottingham in partial fulfilment of the degree of
Master of Research in Geospatial Systems

Word count: 14,877

August 2021

Abstract

Hydropower interacts heavily with river temperature to; meet regulations, maximise profits, and maintain dam safety. Often the operational decisions that dictate this interaction are made without monitoring of river temperature, and so it is proposed that satellite remote sensing may provide a quasi-regular cost-effective method to improve this. This dissertation assesses the viability of using Google Earth Engine cloud computing and Landsat 8 Thermal Infrared satellite measurements to provide actionable insights for hydropower managers. The method was tested in three large rivers (the Saint John River in Canada, the Colorado River in the USA, and the Ganges in India) to assess transferability. No previous study has attempted to extract river temperature from multiple sites in a single study. Three different methods were tested to find the most accurate atmospheric correction algorithm for the task of river temperature measurement. The Statistical Mono-Window algorithm was found to produce the most accurate comparison to kinetic temperature loggers on the Saint John River ($\pm 2^{\circ}\text{C}$) with a R^2 value of 0.96 ($n=40$, $p<0.001$). However, this method was not transferable to the Colorado River indicating application in rivers without validation data should be carried out with caution. A Python Package named SatTemp (Valman, 2021b) was developed to assist hydropower operators in implementing the method along with a dashboard app to disseminate results (Valman, 2021a). Concerns were raised with the “black box” nature of Google Earth Engine and this App, meaning that errors and nuances in the method may be missed. These would need to be addressed before this method can be provided to hydropower operators.

Acknowledgements

I would like to thank the EPSRC for providing a fully funded studentship to enable my research and the Centre of Doctoral in Geospatial Systems for the training and leadership provided, without which this postgraduate study would not have been possible.

I would also like to thank my supervisors, Dr Stephen Dugdale and Professor Doreen Boyd for their encouragement, knowledge, and direction throughout this dissertation.

Finally, I would like to thank my Parents, Deborah and Michael Valman, for their support in getting me to this stage in my studies.

Contents

Abstract.....	2
Acknowledgements.....	3
List of Figures	6
List of Tables	6
List of Equations.....	7
Abbreviations.....	8
1.0 Introduction	9
2.0 Research aims	12
2.1 Aim	12
2.2 Objectives.....	12
3.0 Literature review.....	12
3.1 Water temperature and hydropower operation	12
3.2 Methods of recording and modelling river temperature	15
3.2.1 Modelling	15
3.2.3 Airborne remote sensing methods	16
3.3 Thermal Infrared sensors and emissivity values	17
3.4 Satellite measured river temperature	18
3.5 Analysing satellite imagery	20
3.5.1 Cloud cover	20
3.5.2 temperature extraction algorithms	21
3.6 Cloud computing.....	22
4.0 Method	24
4.1 Introduction to method chapter.....	24
4.2 Input datasets	24
4.2.1 Satellite Sensors	24
4.2.3 Bounding regions	26
4.2.4 Water surface masks.....	26
4.2.5 Cloud Mask Layers	26
4.3 Water surface temperature extraction Algorithms	26
4.3.1 No atmospheric correction	27
4.3.2 Statistical Mono-Window method.....	28
4.3.3 Practical Single Channel method	29
4.4 Processing and visualisation Software	30
4.5 Validating the results	31

5.0 Results.....	33
5.1 Derived water surface temperature maps.....	33
5.2 Interactive App Dashboard	35
5.3 Generation of river temperature long profiles	36
5.4 Validating results using temperature loggers.....	39
5.4.1 Saint John River, New Brunswick, Canada	39
5.4.2 Colorado River, Arizona, USA.....	42
5.6 Atmospheric Correction.....	44
6.0 Discussion.....	46
6.1 Potential and limitations of GEE	46
6.1.2 The SatTemp Python Package.....	48
6.1.3 Easy dissemination: “RiverTemperatureApp”	48
6.1.4 Automation or application of community datasets.....	49
6.2. Relationships between in-situ kinetic loggers and satellite TIR.....	50
6.2.1. Validation statistics	51
6.2.2. Sources of error unique to the Colorado River	52
6.3 Strategies for increasing accuracy	53
6.3.1 Cloud cover improvements.....	54
6.4. Extending river temperature extraction to more rivers	54
6.5 Atmospheric correction and potential.....	55
7.0 Conclusion.....	56
8.0 Reference List.....	58
Appendix A.....	68
Appendix B	72
Project Management Plan	74
Data Management Plan	75

List of Figures

Figure 1: Position of Saint John River kinetic water temperature loggers	31
Figure 2: Position of Colorado River kinetic water temperature loggers	32
Figure 3: Section of the River Ganges used to produce longitudinal diagrams.....	33
Figure 4: Extracted surface water temperature map from the Saint John River, positioned over the Mactaquac dam	34
Figure 5: Example of the sliding map Jupyter notebook for user temperature extraction	35
Figure 6: Screenshot of the RiverTemperatureAPP developed	36
Figure 7: Longitudinal temperature profiles from the Saint John River	37
Figure 8: Comparison of longitudinal temperature profiles on the River Ganges.....	38
Figure 9: Scatter plot of temperature validation using the Saint John River downstream loggers.....	41
Figure 10: Scatter plot of temperature validation using the Saint John River upstream loggers.....	42
Figure 11: Map of erroneous water surface temperature extracted from the Colorado River	43
Figure 12: Scatter plot of lack of correlation found on the Colorado River at in-situ temperature logger 9404200	44
Figure 13: Comparison of atmospheric correction methods correlation coefficients.	45

List of Tables

Table 1: Comparison of Satellite TIR sensors.....	25
Table 2: Statistical MonoWindow algorithm coefficients.....	28
Table 3: Practical Single Channel algorithm coefficients	29
Table 4: Validation results from Saint John River	40
Table 5: Comparison between atmospheric correction methods	45

List of Equations

Equation 1: ToA equation	27
Equation 2: Brightness temperature.....	27
Equation 3: Surface Water Temperature without atmospheric correction	27
Equation 4: Statistical MonoWindow Equation.....	29
Equation 5: Practical Single Channel Equation	29

Abbreviations

Initialism	Description
API	Application Programming Interface
ASTER	Advanced Spaceborne Thermal Emission and Reflection sensor
GEE	Google Earth Engine
GRWL	Global River Width from Landsat dataset
MODIS	Moderate resolution Imaging Spectroradiometer
NAC	No Atmospheric Correction
NCEP/NCAR	National Center for Environmental Protection and National Center for Atmospheric Research
PSC	Practical Single Channel algorithm
SMW	Statistical Mono-Window algorithm
TIR	Thermal Infrared
ToA	Top of Atmosphere radiance
RMSE	Root Mean Squared Error
USGS	United States Geological Survey

1.0 Introduction

Globally, there are many cases of freshwater systems exhibiting a long-term warming trend as a result of climate change (Van Vliet et al., 2013, Kędra, 2020). On a local scale anthropogenic operations have been shown to impact river water temperature by extracting, diverting, or discharging water in the system (Kędra and Wiejaczka, 2018, Olden and Naiman, 2010). This means that river water temperature is a highly dynamic variable and an important social, economic, and environmental resource.

The most obvious example of the multiple entangled factors of river temperature, where different drivers can cool or warm rivers simultaneously, is the construction and operation of dams. On the one hand, dams produce the electrical and economic stimuli for development, especially in isolated rural areas (Shi et al., 2019, Chen et al., 2016), without actively producing carbon dioxide. The lack of greenhouse gasses being produced during operation suggests that dams are 'green' energy (Moore et al., 2010) and as such could help to combat global climate change and therefore river warming. On the other hand, hydropower is not universally seen as a positive tool due to the negative social and environmental consequences entailed, especially for freshwater systems (Wu et al., 2019). One adverse effect is the reduction of river temperature caused by releasing water that is colder than seasonally expected from the bottom of the reservoir (known as the hypolimnion; Daniels and Danner, 2020). This can have serious impacts on fish stocks and other environmental factors by smoothing seasonal water temperature variability (Zhao et al., 2020). Water temperature also influences the safety of dams for humans. Concrete dam structures are more vulnerable to high water temperature and therefore maintenance and safety needs to take this into account (Tatin et al., 2018, Tabari et al., 2020). Similarly, reservoir and downstream drinking water is susceptible to algal blooms or bacterial infections if the water temperature stays too high for too long (Choi et al., 2002), something that requires careful management by dam operators.

The ability to release cooler water from dams (often during the night time), can combat the long-term warming effects discussed and has been "used for decades" (Weber et al., 2017). To some extent, this mitigation can be seen as a driver for the return of dam construction (Boelens et al., 2019), making dams a source of resilience to help adapt to climate change (Ahmad and Hossain, 2020). As a result, local, regional, and national governments currently regulate temperature changes caused by hydropower and other water users to combat the extent of thermal pollution (EPA, 2020) and, to potentially combat the impact of climate change. In the context of hydroelectric power, this dictates how much water can be released and when based on the natural range of seasonal thermal trends expected. In turn this has

financial ramifications for hydropower operators if they constrain water releases (and thus, energy generation) to meet these regulations rather than balancing solely on electrical demand and optimum commercial operation. This in turn also impacts water storage, flood storage and abstraction dynamics of the reservoirs (Ahmad and Hossain, 2020).

For all these reasons it is vital that decision makers, operators and regulators have access to accurate water temperature data to optimise water releases for greatest and safest overall productive gain. However, river temperature is difficult to obtain and is often a neglected variable (Pavelsky et al., 2014), despite its clear importance. While in-situ temperature loggers are placed in some streams to provide accurate, regular temperature values, these are a costly solution that work best on small rivers due to the spatial variability in temperature and the risk of loggers being washed away during high flows. These small streams rarely have sufficient flow for hydropower, with the exception of small run-of-river impoundments that rarely alter temperature (Lange et al., 2018). Temperature data collected by these loggers are often not freely shared, inhibiting their inclusion in hydropower regulatory frameworks (Hannah et al., 2011). Instead, the majority of hydropower facilities currently rely on water temperature as a function of air temperature or use empirical temperature curves to understand the seasonal water temperature regimes of their catchments (Kang et al., 2019, Shi et al., 2021, Tabari et al., 2020, Tatin et al., 2018). Some of these extrapolate from in-situ loggers, but in these cases, they are specific to the dam in question and these models cannot be used elsewhere (Wright et al., 2009). The lack of at-dam water temperature data collection is surprising given the large economic decisions based on these models, particularly so given increasing moves to retrofit Selective Withdrawal Systems (which can extract different temperature water from different reservoir heights to better meet temperature demands; Rheinheimer et al., 2015, Sherman, 2000) to existing dams. Indeed, despite the fact that these installations can be extremely costly (\$100-200 million), the lack of sufficient monitoring means that there is currently no detailed understanding of their effectiveness of financial viability once implemented (Wright et al., 2009). There is therefore an urgent need to develop new methods capable of providing accurate river temperature data for the efficient operation of hydroelectric dams in a world threatened by emissions from fossil fuels.

Here it was proposed that satellite-based thermal remote sensing is now poised to be the opportune way to monitor river temperature for this purpose. The global extent, relatively regular return period, and the large spatial coverage per image make this method ideal for monitoring long-stream river temperature above and below dams (Piégay et al., 2020). Moreover, satellite imagery is increasingly open source, allowing industries and academics to focus on developing specialised algorithms to get the most out of the available data (GEE, 2021e). This is especially true of the Landsat programme, images from which have been

available for free since 2013 (USGS, 2021a) and now include ~4 million thermal images going back to 1984 (He et al., 2018) allowing pre-dam flows to be accounted for. Indeed, Google Earth Engine (GEE) and Cloud Computing mean that it is now theoretically possible for anyone with a standard laptop and internet connection to carry out satellite-based river temperature analysis for anywhere in the world (Gorelick et al., 2017). GEE therefore has clear potential for improving dam operations, particularly in the developing world where data availability has not kept pace with rapid hydropower development (Ahlers, 2020).

Although previous studies have used thermal infrared (TIR) data to extract river temperature data (mostly using techniques pioneered by airborne TIR), these primarily rely on offline/standalone processing of imagery (Ling et al., 2017, Zhao et al., 2020, Yadav et al., 2020, Al-Murib et al., 2019, Xiong et al., 2020). While these examples have demonstrated that it is possible to extract viable river temperature data, such methods are relatively computationally intensive and time consuming. Furthermore, none of these techniques are particularly amenable to the generation of river temperature data for dam operators, who often require quasi-real time access to water temperature data and also rarely have the remote sensing expertise necessary to acquire these data themselves.

Instead, this thesis evaluates the viability of cloud-based methods (i.e., GEE) for the extraction of global river temperature data from Landsat TIR imagery in a manner that is accessible to dam operators. It is proposed that a self-contained user interface could be created utilising GEE and Heroku apps (Danielsson et al., 2021) to produce a dashboard with actionable information for dam operational managers. This would allow river temperature data to be calculated for a chosen catchment with the user only needing to choose the catchment and extraction methodology from a given list without needing to know in-depth information on TIR remote sensing. This draws on the success of HR Wallingford's recent Dam-Sat system (HRW, 2021) which provides independent modules for different aspects of dam safety depending on what the structure requires.

This dissertation will also have a focus on building a method which is transferable to other large rivers globally as this is vital to creating a global ability to measure water temperature. A benefit of providing global coverage is that the results from this study will be transferable to other industries beyond hydropower. Durmayaz and Sogut (2006) used satellite TIR sensors to carry out a suitability analysis for a nuclear power plant. Colder water extracted for cooling would provide efficiency and economic improvements in this scenario. It is infeasible to use in-situ loggers at multiple sites for this purpose, but the method presented here could provide water temperature trend analysis in large rivers to dictate where sewage treatment works, industrial factories or power plants should be placed in order to minimise the costs of meeting

regulations or maximise the efficiency of processes. A rigorous, repeatable, and accurate method for the extraction of global river temperature would therefore be of great benefit for better understanding and monitoring of rivers and the socio-environmental benefits they deliver in a world threatened by climate change.

2.0 Research aims

2.1 Aim

Assess the viability of using Google Earth Engine for the extraction of river temperature outputs for assisting dam and industrial operating procedures globally.

2.2 Objectives

Objective 1: Verify the ability of GEE as a tool for calculating river surface temperature from satellite TIR inputs to produce an interactive tool for extracting river temperature.

Objective 2: Validate the accuracy of the results against different river types to infer the transferability of the method

Objective 3: Compare different atmospheric correction methods to assess which produces the most accurate results

3.0 Literature review

3.1 Water temperature and hydropower operation

Dams have been shown to cool rivers (Daniels and Danner, 2020), an impact which is especially pronounced in summer causing the flattening of seasonal variability (Xiong et al., 2020). The negative impacts on fish and the environment (Heggenes et al., 2018) quickly propagate into social and economic damages. In more developed countries this is mainly found as an impact on recreation and the environment (Chapra et al., 2017). In less developed

countries, where reliance on subsistence fishing is greater (Wu et al., 2019), it can have much more extreme consequences. For example, the world's most productive inland fishery, the Mekong (Jensen, 2001), is under threat from its dams and their current modes of operation (Bonnema et al., 2020). It is estimated that the financial losses as a result of these dams stand at a potential loss of \$500 million a year (Grumbine and Xu, 2011).

However, climate change is driving higher summer air and water temperatures (Liu et al., 2020, Ouellet et al., 2020) which may in part be mitigated by the cooling properties of these dams, if managed appropriately (Kędra and Wiejaczka, 2018). In this context, dams would provide increased resilience for fish stocks by managing rising temperatures (Ouellet-Proulx et al., 2017, Wilby et al., 2010). Environmental Engineering is already used to manage many issues (Board et al., 2019) but with hydropower, careful management and modelling would be required to meet water temperature regulations whilst also maintaining water supplies and profits (Foley et al., 2010). For example, designing operational models around downstream fish stocks without appropriate monitoring can create an unstable reservoir environment harming valuable reservoir fish stocks (Eloranta et al., 2018).

Reservoir level should also be included in water release plans because it can be likened to a large battery (Mäkinen et al., 2020), providing resilience to a power grid that relies on renewable energy (Liu et al., 2019). This facilitates the use of wind and solar energy which are inherently variable (Bloom and Novacheck, 2017). Most models, which show dam operation and help to define power grid policy, "do not comprehensively represent the constraints on hydropower operations" (Stoll et al., 2017). This will be increasingly important due to the need to incorporate climate change and drought into energy production predictions (Meng et al., 2020).

Using water for cooling needs to be accounted for in Production Cost Models. These models define water releases in the short term to meet daily/hourly demand and the diurnal temperature curves (Foley et al., 2010, Shree et al., 2021). Use of water for river cooling also needs to be combined with long term climatic factors. This is done in Capacity Expansion Models which dictate how well a hydropower system will operate in the future (Foley et al., 2010) relying on past and future trends (Xiong et al., 2020).

Part of the difficulty in managing these models is the large number of stakeholders who dictate how much water can be released, when it is released, how much energy is sold, and whose water rights need to be met. Stakeholder research has shown that the provision of information to all parties is a key factor in gaining meaningful and lasting teamwork and success (Wang et al., 2019b). In the past there has clearly been a lack of information sharing, especially in

regard to river temperature (Hannah et al., 2011), making its inclusion in modelling and stakeholder frameworks very difficult.

Balanced operational models require the appreciation of coincident impacts from water releases. Withdrawing too much cold water from a dam reduces dissolved oxygen by causing an upwelling of nutrients encouraging algal blooms (Chapra et al., 2017). In turn this reduces the ability to use dam water for drinking water weakening profit structures and climate resilience (Weber et al., 2017). Algal blooms can also be caused if the reservoir flow is inhibited to the extent that the reservoir warms too much which can also cause cyanobacteria issues (Cha et al., 2017) further damaging drinking water quality (Srinivasan and Sorial, 2011).

Another reservoir temperature concern is dam safety, where temperature and reservoir volume can control displacement and therefore structural stability (Dufour et al., 2015). Temperature profiles change at depth (Pilla et al., 2021) and so does their influence on the structure (Dufour et al., 2015). Only recently have models of dam displacement and safety begun to take this into account (Tatin et al., 2018). Most current models are based on traditional hydrostatic-season-time models developed in the 1960s (Gamse et al., 2018) which assume a perfectly seasonal evolution (Tatin et al., 2018). However, advancing these requires temperature loggers, which as noted are not always available. So these models still often rely heavily or solely on air temperature (Kang et al., 2019). Therefore, the application of satellite remote sensing of water temperature could increase the uptake of these more advanced models and improve dam safety procedures. Whilst attempting to not reduce downstream temperature too much, operators also need to make sure they do not overfill the reservoir causing potential failure (Tabari et al., 2020). Instead, satellite data could feed into existing automated early warning systems and enabling early capacity reduction (Xie, 2021).

The complexity of designing water temperature releases in regard to physical, regulatory, and financial restraints may have contributed to the current lack of uptake in utilising Kędra and Wiejaczka's (2018) work. Therefore, it is important for river temperature releases to be regulated to ensure it is one of the variables accounted for (EPA, 2020). Regulation has been shown to create a positive feedback loop with technological investment which leads to better stringency (Schmid et al., 2020) and it appears as though hydropower is also starting to follow this trend. Change is likely to be less efficient in hydropower than in previous examples (Schmid et al., 2020) due to the construction of dams in pollution havens where environmental regulation is more relaxed (Mulatu et al., 2010). Therefore, technology needs to reduce the complexity of improving water temperature releases to make it feasible globally.

3.2 Methods of recording and modelling river temperature

3.2.1 Modelling

River temperature is primarily collected as a proxy from air temperature (Piccolroaz et al., 2016, Arismendi et al., 2014, Toffolon and Piccolroaz, 2015, Johnson et al., 2021). This has also been done at the global scale (Van Vliet et al., 2013) using climate to predict stream temperature with additional logger data, where available, from UN GEMSTAT dataset (Färber et al., 2018). Although this database holds a lot of records these are often less extensive for river temperature than might be assumed (Van Vliet et al., 2013). These can be used to bounder or show the likelihood of outlier results in the data collected, using expected temperature boundaries (e.g., Mohseni et al., 1998). This is not the most accurate way of measuring temperature and ignores any anthropogenic causes that decouple river temperature from air temperature (Liu et al., 2020).

Models can also be programmed to account for various physical processes which impact river temperature, but these are still limited by the input meteorological data they are based on (Dugdale et al., 2017). This is especially true of some dam temperature models which rely on logger data at a point to understand temperature changes (Voichick and Wright, 2007). These can create effective temperature models for certain tasks but are inherently specific to the catchment they are produced in (Wright et al., 2009). But even in developed countries this limited logger point data is often not available thus returning operators to rely on these air temperature General Linear Models to define release schedules (Weber et al., 2017).

3.2.2 in-situ temperature loggers

In-situ temperature loggers have been implemented in the field for a long time, but the focus has been on smaller rivers (e.g., Johnson and Wilby, 2015). Issues such as the time consumed by checking logger batteries, downloading, and cross calibrating this data (Caissie and El-Jabi, 2020) reduce its effectiveness and uptake by industries in larger rivers. When data is collected there are often issues with data sharing and access especially in developing nations (Hannah et al., 2011) compounding uptake issues. Despite the difficulties associated with placing these loggers in larger rivers, there is a “clear rational for supporting large scale river archives” (Hannah et al., 2011). Including the ability to validate and train models or remote sensing data with highly accurate point data.

Dataloggers have come down in price considerably over the last few decades providing sub hour recordings that operate for a year at a time (Daigle et al., 2017) allowing for networks such as RivTemp consisting of 478 permanent stations (Boyer et al., 2016). However, the claim that this has “democratised” river temperature science (Ouellet et al., 2020) may be premature as the 5 such networks described were all in the more developed Global North.

3.2.3 Airborne remote sensing methods

Expanding the spatial coverage of river temperature measurements through remote sensing has allowed for larger rivers to be monitored and studied (Piégay et al., 2020). This also provides continuous spatial data (Dugdale et al., 2019) enabling the mapping of different temperature zones or longitudinal trend analysis. This is enhanced by the sub-metre accuracy (Dauwalter et al., 2017) which reduces the chance of non-water objects from influencing the results because these will be clearly delineated. This airborne coverage also reduces the need for access which can prevent in-situ temperature loggers being placed in streams and does not suffer the risk of these loggers being swept away or damaged by channel movement (Sowder and Steel, 2012).

Remote sensing of river temperature relies on TIR cameras which are increasingly becoming miniaturised, more effective, and more affordable (Kelly et al., 2019). Mounting these cameras in aircraft is still the most accurate way to produce river temperature (Handcock et al., 2006) and cover a large area but requires a large economic outlay to own, outfit and operate an aircraft (Dauwalter et al., 2017).

Increasingly Uncrewed Aerial Vehicles (UAVs) also known as drones (Dugdale et al., 2019) are being used to provide some of the benefits of airborne remote sensing without the cost associated with aircraft. These are a tenth of the price or less in some cases and can still cover a relatively large continuous spatial area. (Dugdale et al., 2019). These enable increased sampling opportunities as a result of their efficiency but do not have the range to monitor the very large river systems that are most likely to have large dams (Dugdale et al., 2019). By lacking multi-kilometre scale coverage makes them inappropriate for this task, regardless of their ease of use.

Moreover, both UAVs and airborne remote sensing require considerable image pre-processing and reliability assessments to counter drift and environmental conditions (Abolt et al., 2018). In airborne remote sensing this may involve the addition of an expensive GNSS and IMU unit (Johann et al., 2019) or it can require ground control points to georeferenced

images. Both these methods take time and resources meaning that personnel-hours required to record stream temperature through these airborne remote sensing methods are not drastically reduced from those required to implement a logger programme. Without an IMU images may need to be discounted where the viewing angle is low (off Nadir) because an angle of incidence with the water surface which is too high will invalidate results through the reflection of energy.

While these remote sensing techniques collect images over a large spatial extent, remote sensing only acquires a snapshot temporally which makes it very expensive and difficult to maintain quasi-regular recordings (Dugdale, 2016) for use in dam operations.

It is clear that the drawbacks of airborne remote sensing discount it from use in this study based on cost, coverage and return period. Nevertheless, the results produced here should be comparable and interoperable with these higher resolution methods. Enabling the output to be checked with higher resolution at areas of interest or validated against airborne remote sensing results.

3.3 Thermal Infrared sensors and emissivity values

All the airborne methods discussed have been a part of the process developing the hardware and algorithms used with satellite sensors which also relies on TIR cameras. TIR remote sensing utilises the 8-12 μ m wavelength and captures radiant water temperature (Torgersen et al., 2001), this means it is only able to measure the first 100 μ m of the water surface (Abolt et al., 2018). While this may not seem enough to appropriately monitor water temperature it has been shown to correlate strongly to mean water temperature (Handcock et al., 2012). For most tasks this is not needed and instead it is only the comparative difference in water temperature such as above and below dams which is appropriate (Zhao et al., 2020). There is some risk in larger waterbodies with little mixing that thermal stratification, where temperature alters over water depth, may be significant and therefore results will differ from the water column (Daniels and Danner, 2020). However, the majority of rivers have high levels of turbidity which considerably reduces this thermal stratification (Talke et al., 2013).

TIR sensing records the energy emitted by an object. To do this requires a knowledge of the efficiency with which an object emits energy in comparison to a theoretical black body which would absorb all incident radiation and re-emit it perfectly (Handcock et al., 2012). This theoretical black body is given the emissivity value of 1 (Sobrino et al., 2008). The emissivity of water is very close to a black body often found to be around 0.9- 0.98 (Bonnema et al.,

2020, Martí-Cardona et al., 2019). Emissivity can be calculated based on NDVI (Avdan and Jovanovska, 2016) or separate satellite missions (GU et al., 2018) but in rivers it is often assumed to be a constant (Lamaro et al., 2013). This ignores factors such as suspended sediment, roughness of the water surface, and floating vegetation which may have effects on this emissivity value (Handcock et al., 2012) so these may be aspects to consider in the case of unexpected results. All methods that take this emissivity value and the sensor recordings and turn them into river temperature require Planck's Law (Jiménez-Muñoz et al., 2014, Jiménez-Muñoz et al., 2008) which describes the spectral (satellite measured response) of an object based on its emissivity value and temperature (Planck, 1914). Therefore, with a known emissivity value and spectral response, the temperature value can be calculated.

One of the benefits of TIR is that it can be flown at night (Granero-Belinchon et al., 2020) because it measures energy emitted from an object rather than energy reflected from an object during daylight optical remote sensing (Torgersen et al., 2001). However, mixed pixels can produce erroneous values where non-water objects are influencing results (Martí-Cardona et al., 2019). This includes floating algae, moving channel bars and overhanging/shading riparian vegetation. Therefore, airborne remote sensing is usually coupled up with some form of photogrammetry or optical sensor and the benefit of being able to fly at night is rarely utilised especially where it reduces the ability of a satellite to carry multiple sensors.

3.4 Satellite measured river temperature

Satellite TIR has been used for many decades in oceanic studies (Schluessel et al., 1990) but only within the last 10 years has it become a viable option for quasi-regular operational temperature readings (Piégay et al., 2020). The main reasons for this are the increase in freely available satellite data, the increase in computational power, and cloud computing (Zhu et al., 2019, Gorelick, 2013). For example, the United States Geological Survey (USGS) made data from all their missions freely available in 2013 (USGS, 2021a) meaning more scientists could employ it for research.

Satellite TIR imagery can be found at 90m from the ASTER sensor (Despini and Teggi, 2013) and 100m (before resampling) from the Landsat 8 TIR sensor (USGS, 2020). While this is much better than the 1000m pixels returned by the MODIS satellite (Handcock et al., 2012), often used in ocean studies (Díaz et al., 2019) it still limits satellite analysis to the main river branches (Donchyts et al., 2016). The increase in resolution of concurrent optical bands such as the 30m of Landsat 8s Operational Land Imager (USGS, 2020) has provided the ability to better delineate the channel (Yang et al., 2019). This maximises the proportion of streams that

can be measured without pixels becoming mixed by including land and water, which would impact the temperature values returned (Martí-Cardona et al., 2019). There is disagreement over minimum viable river width, with early studies suggesting that just widths of at least 180m would be needed (Handcock et al., 2006) whereas later studies have incorporated alternative bands to produce methods which are claimed to produce viable results at 120m (Martí-Cardona et al., 2019) and 60m resolution (Despini and Teggi, 2013).

Landsat is the most commonly used remote sensing satellite data (Wang et al., 2020a) which is unsurprising given it has a continuous record from 1984 to the present (Young et al., 2017). This record is often longer than traditional data sources available in some river catchments. Being popular has created a positive feedback loop where advice, algorithms, and products (GEE, 2021e, Chander et al., 2009, Young et al., 2017) are produced for Landsat resulting in further advances in its use. Most studies have used the optical sensors and have focused on feature extraction, especially at the global scale (Allen and Pavelsky, 2018, Gardner et al., 2021, Yang et al., 2020). Whereas, in this context, TIR river temperature studies have been restricted to case studies. The importance of dams has already been discussed, and these are often built on large rivers which has led to the majority of satellite river temperature work being centred on this area.

The majority of these papers used Landsat images, downloaded from USGS Earth Explorer (USGS, 2021a) to hard drives and processed in Geographic Information Systems such as ArcGIS (Ling et al., 2017, Yadav et al., 2020, Zhao et al., 2020). This is relatively computationally costly and very time intensive to carry out, leading to studies using very few images (Martí-Cardona et al., 2019). Regardless, the accuracy of this method has been shown to be very high with water temperature matching in-situ records within 0.95°C although this may fall to 2°C for smaller river widths as a result of the aforementioned mixed-pixel problem (Martí-Cardona et al., 2019). The 1000m TIR resolution of MODIS has also been shown to produce reliable results (Xiong et al., 2020) which suggests that large dam systems will be more than accessible with Landsat resolution images. It should be noted that the lack of in-situ data causes some of these studies to not validate their results against known river temperatures creating uncertainty in the literature (Yadav et al., 2020).

Satellite TIR creates the ability to carry out forms of analysis which are considerably more difficult with traditional field studies. For example, longitudinal and temporal trends can be built up utilising the large spatial coverage of satellites (Xiong et al., 2020) and in the case of Landsat the temporal record (Yadav et al., 2020). Moreover, the ability to switch between study sites with ease allows other industries to be considered (Wawrzyniak et al., 2012). Switching between regions without leaving your desktop also allows for suitability analysis to

be carried out. For example, finding a site with the coldest water to increase the efficiency of a planned nuclear plant (Durmaz and Sogut, 2006).

Satellite monitoring at the scale of Landsat and Aster has the additional drawback of only revisiting a site every 16 days which if obstructed by cloud cover (discussed later) can lead to considerable time delays between results. This drawback has been shown to be mitigated by combining modelling with Landsat TIR input images to provide daily stream temperature modelling (Shi et al., 2021). Similarly, satellite data can be used to populate and extend water temperature predictions under future climate change scenarios (Al-Murib et al., 2019) improving the accuracy of these methods.

3.5 Analysing satellite imagery

3.5.1 Cloud cover

Cloud cover obscures satellite images preventing viable results being drawn (Chander et al., 2009). The likelihood of cloud, in an image, changes with region and season meaning some sites are more viable for analysis than others (Armitage et al., 2013). Regardless, there is always potential for cloudy pixels and so methods have been developed to remove them using satellite quality bands, alternative satellite images and ground truthed statistical models (Hollstein et al., 2016).

Using alternative datasets can only work as well as the time period between Landsat and their collection periods (Melchiorre et al., 2020). While ground sensors lack the spatial scale to be useful (Hollstein et al., 2016). Landsat data is supplied with a considerable amount of quality analysis including an estimated scene cloud cover, a simple cloud score algorithm and the “BQA” band (USGS, 2020). Landsat currently uses separate algorithms to determine cloud, cirrus clouds and snow or ice providing a bitwise indication of pixel cloud cover in this BQA band (Foga et al., 2017).

Increasingly machine learning is used to indicate cloud cover, random forests and Bayesian networks have been shown to accurately predict cover with up to 98% accuracy (Hollstein et al., 2016). Originally, these were less simple to implement than common decision trees, but they have been incorporated into the EEMont package (Montero, 2021) and so can also be applied to Landsat data.

Multiple possibilities are available for cloud reduction and the best use case has to be chosen for the desired outcome. Increasing the computing required by using an intensive machine learning technique may be worthwhile to gain a few percentages better cover if values are

being extracted from a point. But if thousands of pixels are being viewed on a visualisation it may be better to rely on the provided quality bands when erroneous pixels will clearly be visible when surrounded by cloud free pixels.

3.5.2 temperature extraction algorithms

To convert TIR sensor data from the digital numbers that are supplied by the Landsat satellite to water surface temperature requires a number of steps (Young et al., 2017). Firstly, this involves conversion from the at sensor digital number to a Top of Atmosphere (ToA) value (Chander et al., 2009) which uses band specific constants consistent across time and position meaning it can be provided as a pre-processed product (USGS, 2020) for all Landsat images.

When using Landsat 8 there are two choices which define the algorithm used to extract river surface temperature from ToA radiance. Firstly, there are two TIR Bands provided by Landsat 8 with the intention of facilitating split-window algorithms using both Band 10 and 11 (Jiménez-Muñoz et al., 2014) which had the potential to provide the most accurate results when using artificial data (Rozenstein et al., 2014). However, the choice of band is negated by a calibration uncertainty within the sensor, called the stray light phenomenon (Montanaro et al., 2014). This stray light issue affects band 11 considerably more than band 10 therefore it is recommended not to be used (Barsi et al., 2014, Ermida et al., 2020). There have been attempts to correct for this error, (Montanaro et al., 2015) however, the conservative choice is to use single channel algorithms only using band 10.

In some sense it is claimed that using Band 10 alone is preferable due to the narrow wavelength excluding the 12 μm region, where absorption and emission from water vapour is higher, thus improving retrieval performance (Ermida et al., 2020). These single channel algorithms then need to choose if and how they account for the atmosphere and provide a mathematical correction for it or not (Wang et al., 2020b). It is possible to not account for the impact of the atmosphere and still get values within 3°C of near-surface temperature which introduces further error from actual ground temperature (Avdan and Jovanovska, 2016). To some extent this can provide a base measure to compare atmospherically corrected methods to, although it is likely to be less efficient where air-water moisture is higher (Wang et al., 2020b).

There are four main categories of atmospheric correction method, the radiative transfer method (Lamaro et al., 2013, Jiménez-Muñoz et al., 2008) used by the majority of the dam studies described. This has previously not been possible in GEE because it requires a

complex radiative transfer model (Barsi et al., 2003) which was previously not available to be batch processed. Upwelling radiation, Downwelling radiation and Transmissibility which this model provides are now available on a pixel-by-pixel basis with the Landsat 8 collection 2 pre-processed data (USGS, 2020). This enables an improvement on the centre of scene method employed by previous studies (Ling et al., 2017) but a method is still being developed to implement a radiative transfer model in GEE or other cloud computing software.

The other three methods; Mono-Window algorithms (Qin et al., 2001, Ermida et al., 2020), Generalised single-channel algorithms (Jiménez-Muñoz and Sobrino, 2003) and Practical Single Channel (PSC) algorithms (Wang et al., 2020b) all employ atmospheric parameters such as water vapour to calculate atmospheric effects. The Statistical Mono-Window (SMW) algorithm (Ermida et al., 2020) and PSC (Wang et al., 2020b) have both been presented as a GEE workflow to allow global land surface temperature modelling. The PSC algorithm is proposed to be the most effective (Wang et al., 2020b), marginally more effective than the SMW algorithm. Both the SMW and PSC algorithms relying on the National Centres for Environmental Prediction-Global Reanalysis dataset to provide air water moisture content. It has been argued that the Modern Era Retrospective-Analysis for Research and Applications data produce less bias (Meng and Cheng, 2018), but this is unavailable on the GEE platform.

Neither the SMW nor the PSC algorithm were explicitly validated against water surface temperature so it is unknown how well these will operate in the context of an object with a very high emissivity. Moreover, both these methods were written for the JavaScript GEE platform which is effective and can be considered more user friendly but lacks the ability to batch process images and sites that the Python platform has. Thus, in their present form these methods are not as transferable or usable as they have the potential to be.

3.6 Cloud computing

One of the main limitations of satellite remote sensing is the considerable computational power needed to manage a large number of images (Tamiminia et al., 2020). Cloud computing has provided an opportunity to circumvent this by moving the majority of processing tasks to a server and negating the need for a client to download images (Gorelick, 2013). Part of the processing speed increase is caused by any calculations or resampling not being carried out until data are requested to be displayed. This provides the ability to access vast quantities of data very quickly making interactive maps in GEE apps feasible (GEE, 2021a) for engineers and scientists to interrogate (Perkel, 2018).

This increases the speed and versatility of remote sensing procedures and has the additional benefit of making it viable for anyone with a link to the internet to use (Gorelick et al., 2017). There is some disagreement about the disconnect between potential uptake of GEE and its actual use in less developed countries (Kumar and Mutanga, 2018). There is also some debate over the Open-Source nature of GEE because if it is utilised by industry, it requires a licence fee paid. Regardless, it has still been influential in well-funded institutions during the pandemic where access to high power computing may have been limited (Alashhab et al., 2021).

Whether carried out on the cloud or with local computing, calculation and extraction of TIR requires a number of steps which should be automated to minimise this risk of user error (Avdan and Jovanovska, 2016). This can be done with tools such as model builder in ERDAS imagine (Avdan and Jovanovska, 2016) or ArcGIS model builder (ESRI, 2016). Although few papers mention this in the methodology it is assumed that they undergo the same process. The open-source alternative is to script the automation of this using a programming language.

GEE allows access to its servers via either a JavaScript or a Python Application Programming Interface (API) (GEE, 2021c). Both these APIs promote knowledge exchange by allowing the sharing of scripts (Mutanga and Kumar, 2019) reducing development time for new projects and providing the ability to check results. While there may be more JavaScript users due to the user-friendly code editor (GEE, 2021c) the Python API does not have a single preferred visualisation method. The Python API is that it allows GitHub and PiP (Valman, 2021b) based open-source package creation. These packages can drastically improve the useability of the product and can be advanced to solve problems required (Montero, 2021, Wu, 2020).

While satellite TIR Riverine papers generally used less than 100 images (Yadav et al., 2020, Ling et al., 2017, Al-Murib et al., 2019) and as few as 6 (Martí-Cardona et al., 2019) by employing GEE it has been possible to carry out a study with as many as 1364 images (Bonnema et al., 2020). The main part of the GEE process that makes this possible is the removal of the need for vast data storage (Wang et al., 2018) where a single band of a single Landsat scene may otherwise account for 108mb of disk space which adds up very quickly (USGS, 2021a). The ability to process large quantities of data at speed has allowed the construction of algorithms which can be applied globally (Ermida et al., 2020, Wang et al., 2020b).

4.0 Method

4.1 Introduction to method chapter

A Python cloud computing function was developed to measure satellite derived river surface water temperature which allowed a choice of three different atmospheric correction methods. Results were validated using in-situ loggers in the Saint John River, Canada. From this the most effective atmospheric correction method was validated against two more rivers to test its ability in different areas of the globe with different river types. The results were visualised through maps, longitudinal diagrams and an interactive mapping app to meet objective 1; assessing the use of GEE as a tool.

4.2 Input datasets

4.2.1 Satellite Sensors

The Landsat 8 Collection One TIR product flown by NASA and the USGS (USGS, 2019b) was chosen to provide input data and was accessed via the GEE catalogue (GEE, 2021b). This provides a global land coverage with a 16-day return period, from April 2013 when it achieved operational orbit to present (USGS, 2019b). This choice ensures the opportunity for methods to be applicable in future research due to the continuance of the Landsat missions with a planned launch of Landsat 9 in fall 2021 (Masek et al., 2020). All methods developed here can be extended to previous TIR Landsat missions (starting from Landsat 4 in 1982; USGS, 2018). Thus, potential future temporal extent is the main reason Landsat was chosen over ASTER TIR which provides a similar resolution and return period (Table. 1). The raw digital numbers provided by Landsat sensors need to be converted through a number of steps to produce river water temperature (Jiménez-Muñoz et al., 2014). However, Landsat sensors have a relatively narrow field of view meaning they do not need to factor view angle into these calculations unlike airborne remote sensing.

Table 1: Statistics of thermal infrared satellites available for this study from which Landsat 8 was chosen. The Landsat missions no longer recording were excluded from the study, however they are included here to provide evidence of the temporal statistics possible if the study was extended

Satellite/sensor name	Band(s)	Wavelength (μm)	Resolution (m)	Return Period	Start and End of recording record	Reference
Moderate Resolution Imaging Spectroradiometer (MODIS)	31	10.78-11.28	1000	1-2 days	February 2000 to present	(USGS, 2021c)
Advanced Spaceborne Thermal Emission and Reflection Radiometer (ASTER)	10	8.125-8.475	90	16 days	March 2000 to present	(Abrams, 1999)
	11	8.475-8.825	90			
	12	8.925-9.275	90			
	13	10.25-10.95	90			
	14	10.95-11.65	90			
Landsat 8	10	10.6-11.19	100m*	16 days	April 2013 to present	(USGS, 2019b)
	11**	11.5-12.51	100m*			
Landsat 7	6	10.4-12.5	60m*	16 days	January 1999- July 2021	(USGS, 2019a)
Landsat 5	6	10.4-12.5	60m*	16 days	January 1984- May 2012	(USGS, 2018)
Landsat 4	6	10.4-12.5	60m*	16 days	August 1982- December 1993	(USGS, 2018)

* Resampled to 30m

** Recommended not to be used due to stray light calibration errors

4.2.3 Bounding regions

WWF HYDROSHED data, also available from the GEE data catalogue, were used to constrain the satellite image and therefore rivers selected. The method was adaptable to alternative bounding geometries but the benefit of the HYDROSHED system is that it is based on catchment area. Dams may cause premature division to the HYDROSHEDs catchments due to their influence on the topography, which makes them useful for dividing the up and downstream catchments.

4.2.4 Water surface masks

To produce reliable results pure water pixels are needed and therefore results should have a water mask placed on them. Here the Global River Width from Landsat (GRWL; Allen and Pavelsky, 2018) was used to constrain channel width to reduce the development time of extracting water masks. 30m Optical bands from the Operational Land Imager sensor also flown on Landsat 8 make it possible for more traditional water masks such as the Normalised Difference Water Index to be added to the method in future experiments.

4.2.5 Cloud Mask Layers

Cloud masking was required to remove pixels effected by cloud, shadow or cirrus which would otherwise cause erroneous results. These errors can be quite extreme, prompting some studies to remove pixel values below 0°C (Bonnema et al., 2020) instead of predicting cloud cover. However, the BQA band provided with Landsat raw images allows optimisation of cloud removal without considerable additional processing requirements (USGS, 2019b). A Bitwise function was used here to remove the affected pixels based on this BQA band.

4.3 Water surface temperature extraction Algorithms

Three methods of extracting water surface temperature from satellite images were implemented to test which was most accurate. These were all single channel methods, one with no atmospheric correction (NAC), a Statistical Mono-Window (SMW) algorithm and a Practical Single Channel algorithm (PSC). As discussed in the literature review, the stray light

effect recommended against split window algorithms (Ermida et al., 2020) and other methods required datasets not available in GEE (Wang et al., 2020b).

4.3.1 No atmospheric correction

The NAC method produced originally in ERDAS IMAGINE (Avdan and Jovanovska, 2016) provides a control result to compare with other methods. As with the other methods, this requires a conversion from digital number to ToA spectral radiance (eq.1). This can be carried out using the built in GEE algorithm (GEE, 2021e) or by using the pre-calibrated ToA dataset provided by GEE. However, there was a lack of clarity in the GEE metadata (See discussion) which led to the conservative approach of calculating ToA from raw values. The resulting spectral radiance was then converted to at-sensor brightness temperature, again relying on band specific parameters (eq. 2). Finally, using Plancks equation the emissivity value of water was included in order to extract river water temperature (eq. 3). A constant emissivity value of 0.991 was adopted for all methods (Martí-Cardona et al., 2019)

$$L\lambda = \mathit{gain} * \mathit{DN} + \mathit{bias} - O_i$$

Equation 1: Where *gain* represents the band-specific multiplicative rescaling factor, *DN* is the raw image digital number values, *bias* is the band specific additive rescaling factor and *O_i* is the correction for Band 10 (Barsi et al., 2014).

$$BT = \frac{K_2}{\ln \left[\left(\frac{K_1}{L\lambda} \right) + 1 \right]} - 273.15$$

Equation 2: Where *BT* is Brightness temperature, *K₁* and *K₂* are band specific thermal constants.

$$\mathit{Water Surface temperature} = \frac{BT}{1 + \left[\left(\frac{\lambda BT}{\rho} \right) \ln(\epsilon) \right]}$$

Equation 3: Where λ is the wavelength of emitted radiance, for which 10.895 was used (Markham and Barker, 1985), ϵ is emissivity and ρ is a constant based on the Boltzmann and Planck's constants (Avdan and Jovanovska, 2016).

4.3.2 Statistical Mono-Window method

The SMW algorithm developed by (Ermida et al., 2020) takes advantage of the already calibrated ToA Landsat datasets provided by GEE (GEE, 2021b), although this does not include the correction factor O_i in equation 1, it was decided to assess the quality of the SMW method required keeping to the process defined by Ermida et al. (2020).

SMW linearises the radiative transfer equation and then assumes the different radiative values based on the relationship between air water moisture and this linearised equation. The linearised equation compared total column water vapour from the National Center for Environmental Protection and National Center for Atmospheric Research (NCEP/NCAR) dataset and radiative transfer values. The initial calibration of this linearised equation was not required as the results were made available in the open-source code (Table. 2; Ermida et al., 2020). For each of ten possible classes for air water moisture, three coefficients were provided (Table. 2) which fed into the following equation to turn ToA brightness temperature into Surface water temperature (eq. 4).

Table 2: Coefficients of the linearised radiative transfer equation used by the SMW method based on Air Water Moisture values (Ermida et al., 2020). Note: Coefficient B (4.2-4.8cm) is does not follow the increasing trend, which may be an error by Ermida et al. (2020).

Total Column Water Vapour (cm)	Coefficient A	Coefficient B	Coefficient C
0-0.6	0.9751	-205.8929	212.7173
0.6-1.2	1.0090	-232.2750	230.5698
1.2-1.8	1.0541	-253.1943	238.9548
1.8-2.4	1.1282	-279.4212	244.0772
2.4-3	1.1987	-307.4497	251.8341
3-3.6	1.3205	-348.0228	257.2740
3.6-4.2	1.4540	-393.1718	263.5599
4.2-4.8	1.6350	-451.0790	268.9405
4.8-5.4	1.5458	-429.5095	275.0895
>5.4	1.9403	-547.2681	277.9953

$$\text{Water Surface Temperature} = A_i \frac{Tb}{\varepsilon} + B_i \frac{1}{\varepsilon} + C_i$$

Equation 4: Where A_i , B_i and C_i are the coefficients based on NCEP/NCAR water vapour dataset values. Tb is Top of Atmosphere brightness and ε is the constant emissivity value of 0.991 chosen.

4.3.3 Practical Single Channel method

In previous studies over land the PSC method has been shown to work better than the SMW method (Wang et al., 2020b). Both were included to compare their ability to extract water surface temperature and to give users more choice within the package created. This method is similar to the SMW in a lot of ways but has 8 constants (Table. 3) per satellite band (Landsat 8 Band 10 in this study) which are entered into Planck's equation with Air Water moisture Equation 5; Wang et al., 2020b, Wang et al., 2019a).

Table 3: Coefficients of Planck's model used in the Practical Single Channel method for Landsat 8 band 10 (Wang et al., 2020b).

Coefficient	value
a_0	-0.4107
a_1	1.493577
a_2	0.278271
a_3	-1.22502
a_4	-0.31067
a_5	1.022016
a_6	-0.01969
a_7	0.036001

$$\text{Water Surface Temperature} = \frac{C_2/\lambda}{\ln\left(\frac{C_1}{\lambda^5 * B(T_s)} + 1\right)}$$

$$\text{With } B(T_s) = a_0 + a_1w + (a_2 + a_3w + a_4w^2)\frac{1}{\varepsilon} + (a_5 + a_6 + a_7w^2)\frac{L_{sen}}{\varepsilon}$$

Equation 5: Where L_{sen} being at-sensor radiance, ε being the constant emissivity of 0.991 chosen, w is the air water vapor content, constants C_1 and C_2 equalling $1.19104 \times 10^8 W\mu m^4 m^{-2} sr^{-1}$ and $1.43677 \times 10^4 \mu mK$ respectively, $B(T_s)$ is Planck's radiance using a_{0-7} from Table 3 and λ is the effective wavelength of $10.904\mu m$.

4.4 Processing and visualisation Software

GEE cloud computing was used to process Landsat Images from the GEE data catalogue using the algorithms described above. This open-source system allowed for images to be used without the need to download them and reduced processing and resampling to their minimum requirements for the visualisation or data download required. This meant that the entire project could be carried out on a relatively affordable 64 bit laptop with internet connection and did not need a high-powered machine or access to a computer lab.

This process was carried out with the Python API in Jupyter Notebooks, using the GEEMap package for visualization (Wu, 2020). Using the Python API over the JavaScript API meant that batch processing quantities of data from different sites was feasible due to the ability to run cells successively reducing processing time and data limitation errors.

GitHub and PIP were used to produce a packaged version of the method (Valman, 2021b) so it could be employed by other developers and researchers without the need to copy code. The package was created in the Spyder Python API (Spyder, 2021) because although Jupyter Notebooks is effective for visualisation and development it is not capable of providing package support.

QGIS 3.16.5 with the GRASS 7.8.5 extension was employed to vectorise a channel centreline when the GRWL centreline product (Allen and Pavelsky, 2018) was seen to not be accurate enough for this task. The “v.to.points” tool was used to place points every 100m on this channel centreline vector and then the raster to points tool was used to extract values for a longitudinal temperature plot.

Additional Python packages GeoPandas and Pandas were required to georeference the point locations required to validate this study (McKinney, 2010). Numpy and Scipy packages were required to calculate the statistical success of validation measures (Harris et al., 2020, Virtanen et al., 2020). Finally, the Matplotlib package was used to visualise the validation results and longitudinal diagrams (Hunter, 2007).

An App based dashboard (Valman, 2021a) was created using Heroku and GEEMap which allowed for a direct interactive display of the method to be available online without the need to apply programming (Wu, 2020). Ipywidgets were used to provide functionality around this product (Munk and Turk, 2020).

4.5 Validating the results

The three different algorithms to extract river temperature were first tested to see how well they performed at predicting the river water temperature of the Saint John River, New Brunswick, Canada. Kinetic stream temperature logger records from 2014 and 2015 using HOBO UA-002-64 (Dugdale et al., 2018) were compared to results from each atmospheric correction method at 6 locations (Figure. 1). With widths ranging from 330m to 840m making edge effects unlikely to impact channel centreline satellite results, thus making this a good case study site.

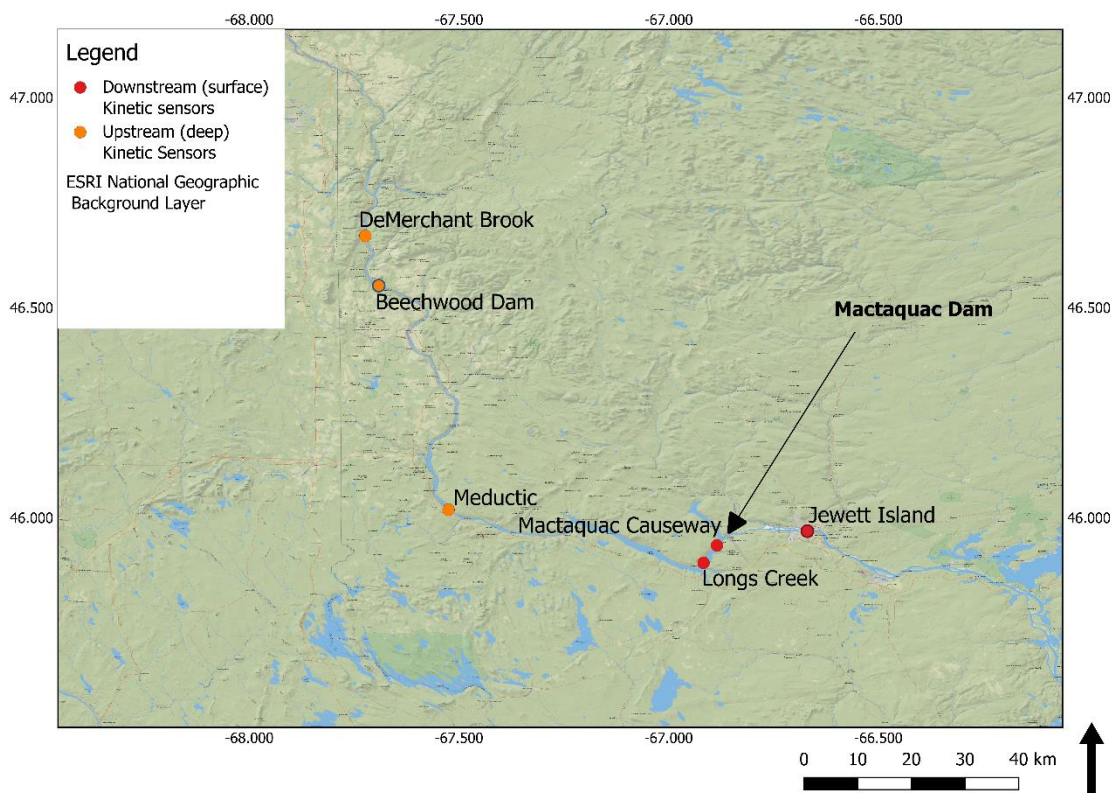


Figure 1: Location of in-situ monitoring locations, 2014-15 used for the study. Red locations are clustered around the Mactaquac dam and are surface kinetic temperature loggers, while the orange locations further upstream represent deeper loggers with which were in place for less time.

As noted, the literature claims that mixing within riverine systems is significant enough to account for thermal stratification which causes the water surface temperature to differ from temperature at depth (Talke et al., 2013). This was checked here by the inclusion of the upstream loggers which were placed at a deeper depth and compared separately.

Local time deltas in the results were converted to Greenwich Mean Time which is the same as the Zulu time Landsat operates on. Values were then extracted using all three temperature algorithms and matched for date and time. The accuracy of these different algorithms was measured using Root Mean Squared Error (RMSE), Bias and Pearson's correlation test. Scatter graphs were also created to check results met the linear requisite of Pearson's test. Finally, Fischer's Z test was used to compare the different correlations to analyse if they were statistically significantly different.

The most effective validation method was trialled in two other rivers to test its ability to respond to different river systems and climate zones. There is a paucity of freely available in-situ temperature measurements which played a large part in dictating the choice of river.

The Colorado River, below Glen Canyon Dam, Arizona USA provided a river running through a desert climate with water temperature that fluctuate between 0 and 30°C (Voichick and Wright, 2007). StowAway XT132 and HOBO H2O logger results were provided by the Grand Canyon Monitoring and Research Center (USGS, 2021b) and run consistently throughout the Landsat 8 recording period (Figure. 2). River widths ranged from 85m to 200m which enabled testing of the minimum river width appropriate for satellite TIR monitoring.

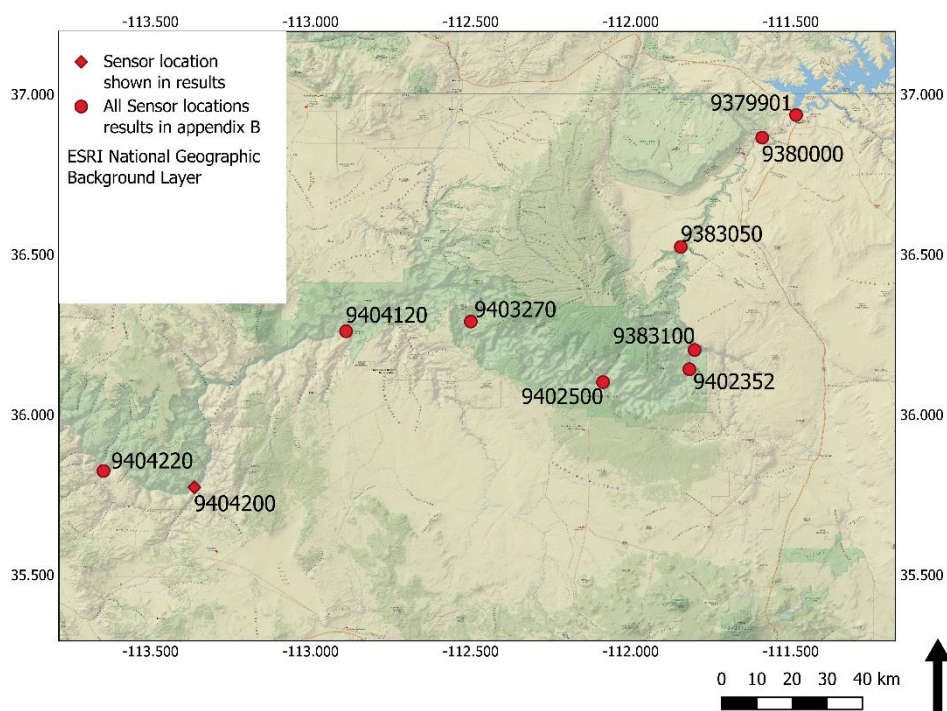


Figure 2: In-situ temperature logger positions on the Colorado River, Arizona, USA. Only the results from logger 9404200 as it produces the strongest correlation between satellite sensing results and observations, but all other results are presented in Appendix B.

In lieu of available temperature logged data, results from the method were also validated against previous satellite TIR studies on the River Ganges (Figure. 3). Longitudinal diagrams

were created for February 2015, 2017, and 2018 and compared to those in the Yadav et al. (2020) study. This allowed assessment in direct comparison to other methods as well as the ability to test the method in an Asian glacial and monsoon fed river. All Landsat 8 images used in this study can be found in Appendix A with some of their metadata.

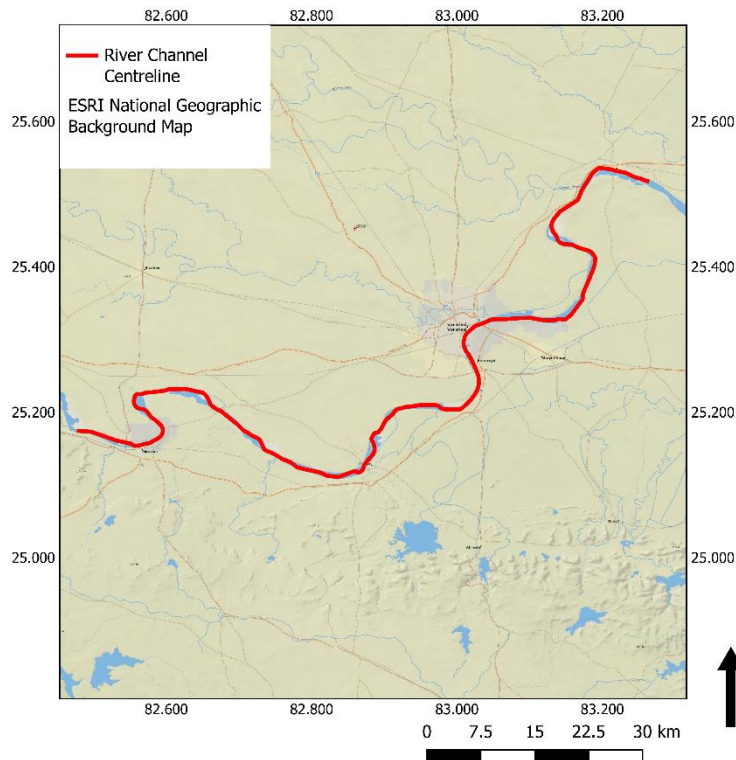


Figure 3: Centreline of the mid-portion of the River Ganges near the city of Varanasi, where longitudinal profiles were calculated using the method presented here and by Yadav et al. (2020).

5.0 Results

5.1 Derived water surface temperature maps

GEE was shown to be a capable of calculating and producing river temperature visualisations and results from Landsat 8 imagery (which has some potential to subsequently be used by hydropower operators; Figure. 4). These visualisations allowed for the selection of a WWF HYDROSHEDs Watershed geometry relevant to the user and then the calculation of river

temperature for all stream segments which intersected this geometry (Figure. 5). The method allowed for any number of Landsat 8 images between April 2013 and the present to be selected and their river temperature data extracted; the full list of the 156 Landsat scenes and their metadata used in this study are available in appendix A.

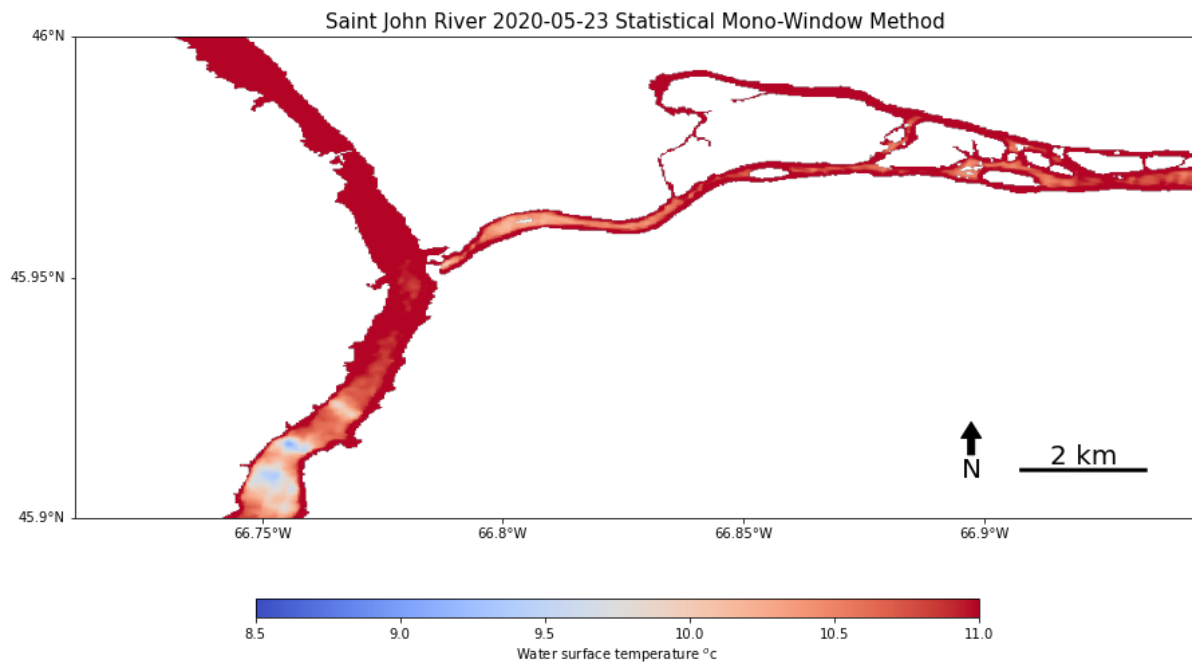


Figure 4: Surface water temperature output for Saint John River, New Brunswick, Canada on 23rd May 2020 (using the Statistical Mono-Window method and the GEEMap/Jupyter Notebook visualisation tool). The image is downstream of the Mactaquac Dam (near Fredericton, New Brunswick) and could be compared to expected temperatures or areas of interest as the dam operators wished. Missing pixels exist where the cloud cover algorithm has removed them.

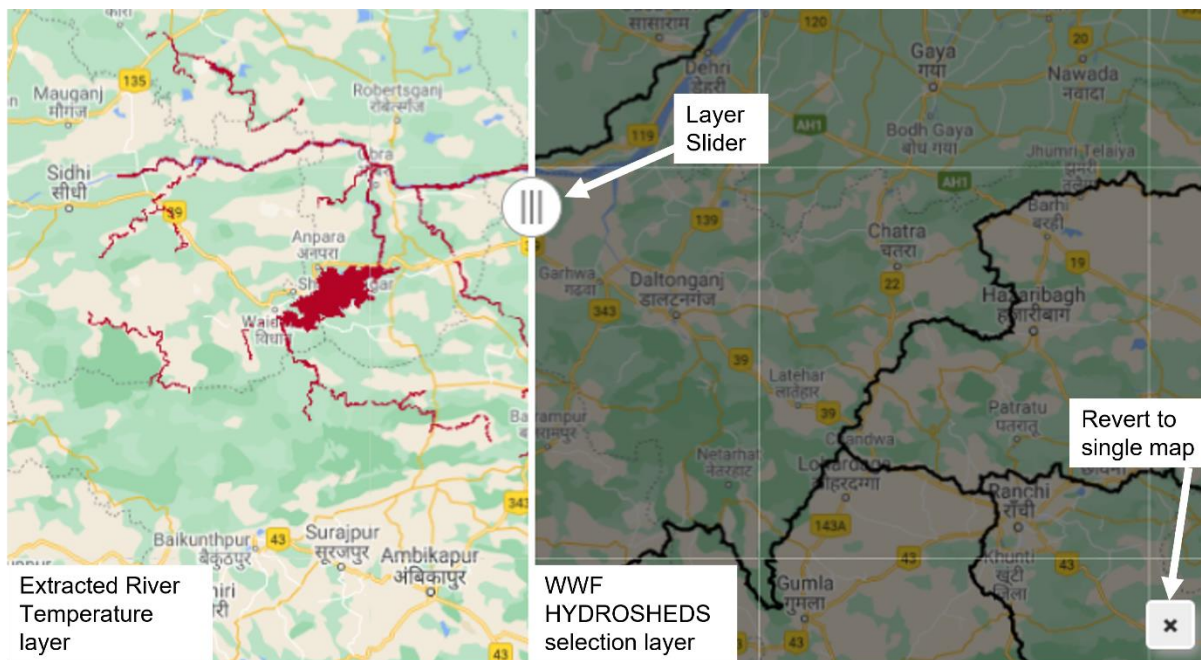


Figure 5: An example of the interactive sliding map in the Ganges River basin. On the right a WWF HYDROSHED River basin can be interrogated for its ID which is then fed into the left-hand map. The slider can then be pulled across to visualise the same site with the river surface temperature calculated using the Statistical Mono-Window method. In this case on the 08th of June 2015. Note the cross, bottom right, which converts this split map into a single map once the WWF HYDROSHED is no longer needed.

5.2 Interactive App Dashboard

An interactive dashboard was created (Valman, 2021a) to display river temperature to a user without expertise in programming or GEE. The dashboard has widgets which allow the user to select a date range, atmospheric correction technique and alter the image symbology (Figure. 6). These widgets are customisable and therefore additional functionality can be built in, including graphs and options to change the map position. The built-in functionality of GEEMap allows the user to interrogate pixels or build a histogram over a drawn transect making it viable for a variety of purposes.

River Surface Temperature using Google Earth Engine and Landsat 8

Use the spanner button (top right) and the inspector tool to find the values of any pixels

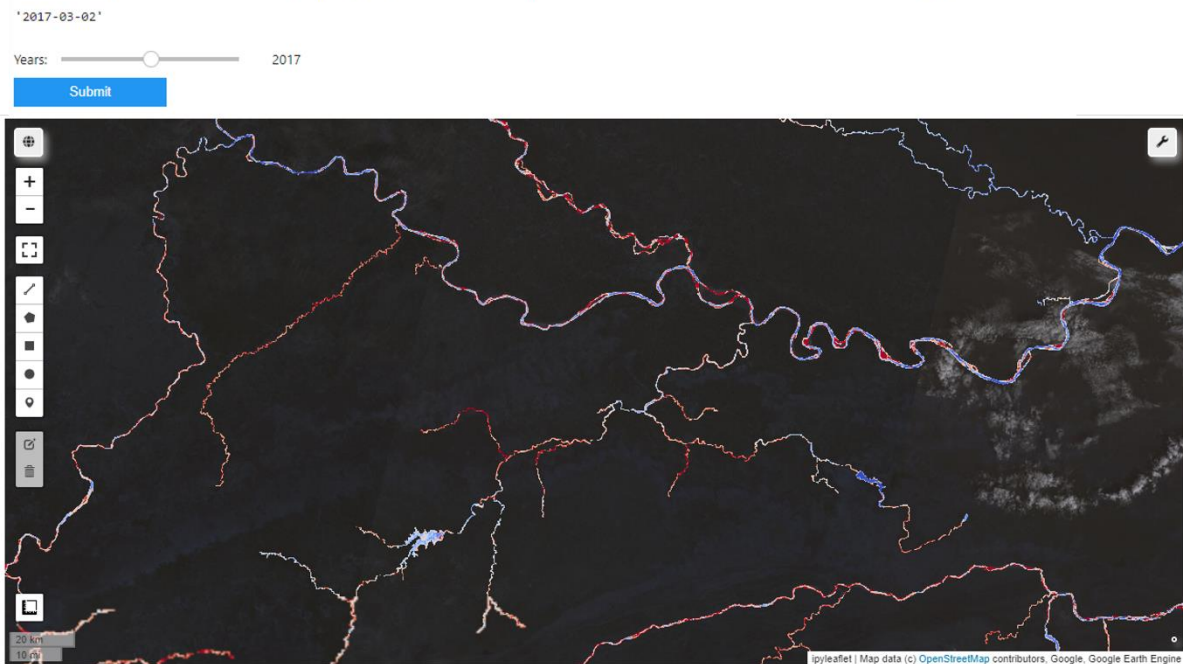


Figure 6: A screen grab of the interactive dashboard (Valman, 2021) which is displaying river surface temperature from the Ganges Basin on the 2nd March 2017. Functionality can be added and removed from this app to specialise it for different users.

5.3 Generation of river temperature long profiles

When combined with QGIS, the GEE method was shown capable of generating longitudinal river temperature profiles which can provide a useful output to understand impacts of a dam on the upstream and downstream reaches of a river, along with how far the dam's impact persists downstream (Figure. 7).

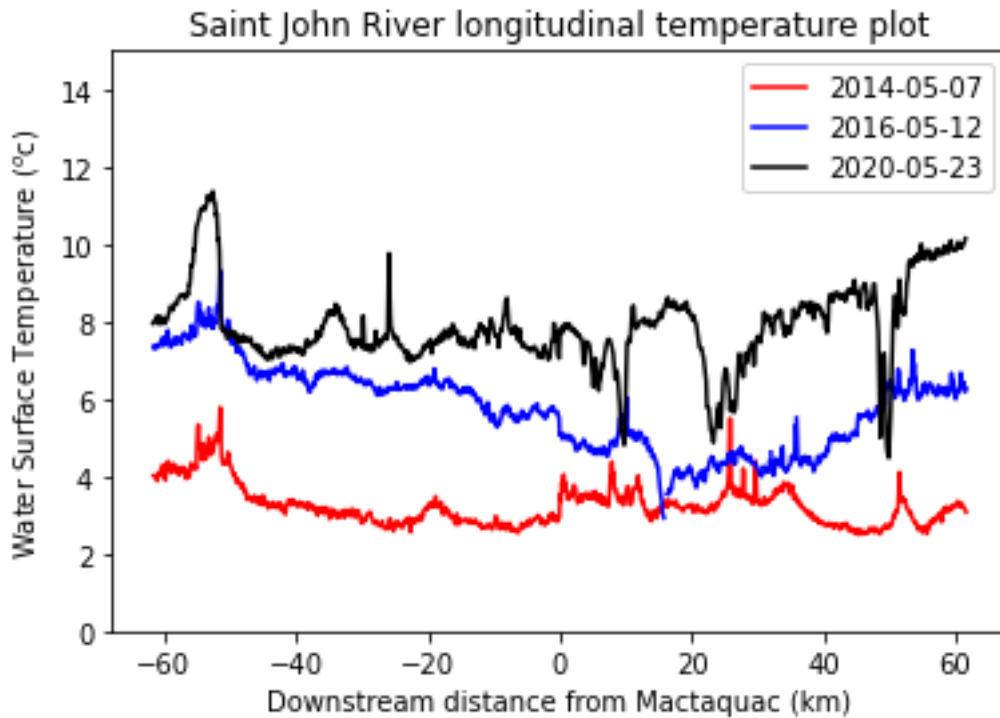


Figure 7: Longitudinal profile of Saint John River, New Brunswick, Canada on 23rd May 2020 using the Statistical Mono-Window Method. Values extracted every 100m from the channel centreline measured from the Mactaquac dam. Temperature 'spikes' values are likely the result of in channel bars or shallow warmer zones.

The application of longitudinal profile diagrams in India (Figure. 8a) also allowed some subjective validation against previous satellite TIR studies (Yadav et al., 2020; Figure. 8b). This was carried out because there was no in-situ logger data in a large river in a developing country that could be accessed for use in this study. The method used here was shown to produce similar results to the temperature values produced by Yadav et al. (2020) especially with regards to the 4°C difference between images collected in February 2015 and February 2017. Results show a different bias to those produced with the radiative transfer method but without logger data it is difficult to know which is more accurate. The results produced here do show more extreme values than those produced by Yadav et al. (2020), possibly as a result of the use of a single centreline delineated using the 2015 Landsat image which was not changed and therefore did not account for channel change. Yadav et al. (2020) delineated new channel centrelines for each image date reducing the impact of channel change.

River Ganges longitudinal temperature plot

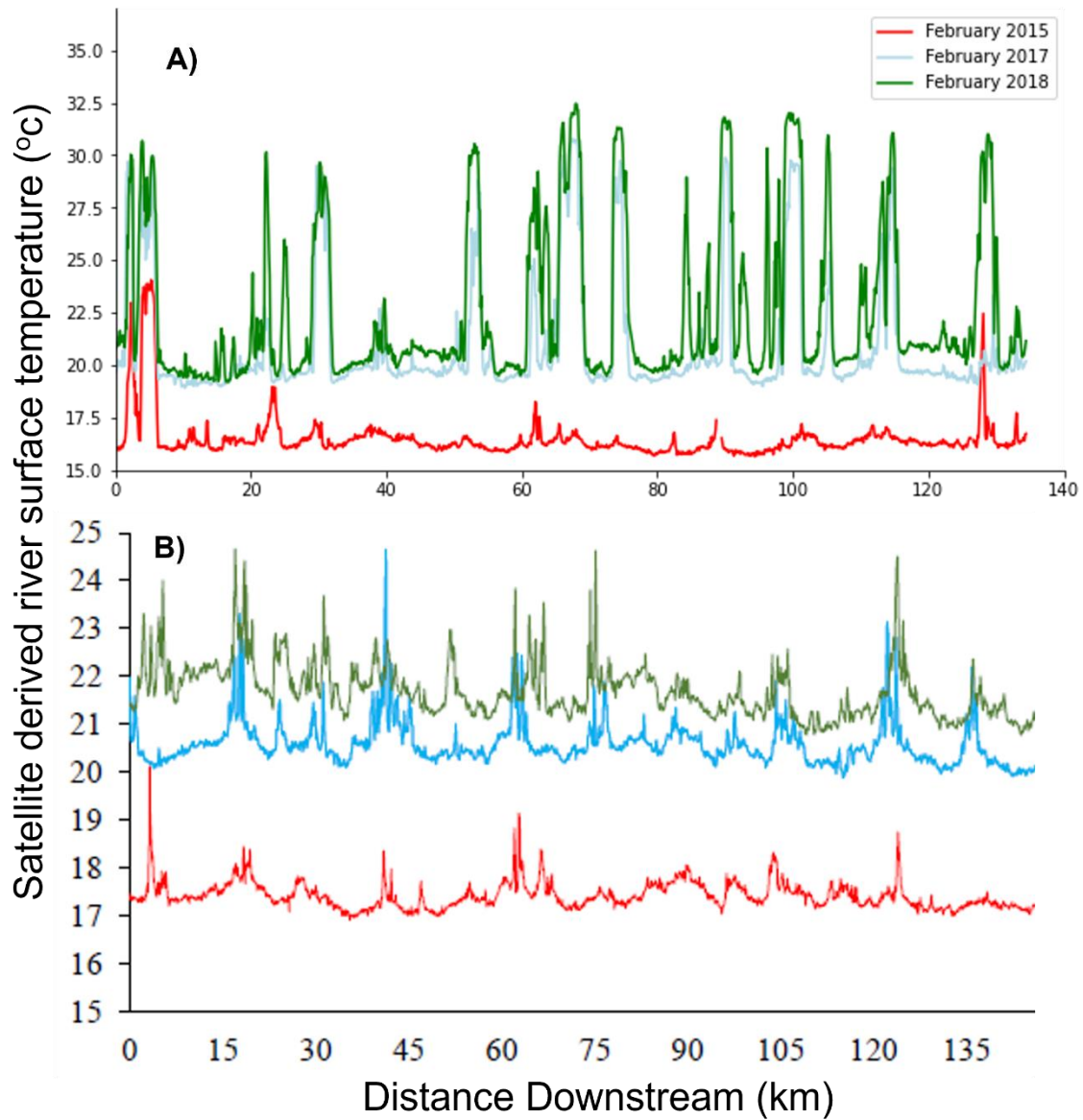


Figure 8: Comparison of longitudinal river temperature analysis carried out on the Ganges. Plot A employs the Statistical Mono-Window method in Google Earth Engine and uses one centre line vectorised on QGIS over the February 2015 results. Plot B is from (Yadav et al., 2020) and utilises ArcGIS and the radiative transfer method. The increase in extreme values in plot b in comparison to plot A is attributed to changes in river planform over time in a highly dynamic stream and infers a new centre line would be needed for each Landsat image.

5.4 Validating results using temperature loggers

5.4.1 Saint John River, New Brunswick, Canada

A more informative validation was carried out on the Saint John River, New Brunswick between July 2014 and December 2015 using in-situ (kinetic) stream temperature data acquired at a series of locations using HOBO UA-002-64 temperature loggers (Dugdale et al., 2018). Significant strong correlations between temperature logger values and satellite observations (Table. 4) at all sites (as evidenced by high R^2 values). RMSE ranged between 1°C and 5 °C degrees with a negative bias found across most sites (Figure. 9). Some loggers further upstream were placed at a greater depth and were included to test the robustness of the method. These also produced relatively strong correlations (Figure. 10) although they had a larger RMSE (Table. 4).

Table 4: Validation statistics comparing the results of different atmospheric correction methods on the St Johns River. NAC stands for the Non-Atmospherically Corrected method (Avdan and Jovanovska, 2016), SMW stands for the Statistical Mono-Window algorithm developed by (Ermida et al., 2020) and PSC is the Practical Single Channel method developed by (Wang et al., 2020b). N relates to number of satellite images/dates and differs between methods due to availability of atmospheric datasets needed for the PSC method. Pearson's R tests were applied to test for correlation and the significance of this correlation. Validation results from Saint John River

Temperature logger site	NAC	SMW	PSC
Jewett Island			
n	13	13	13
R ²	0.970	0.967	0.860
P-score	<0.001*	<0.001*	<0.001*
Bias	-5.42	-0.676	-5.69
RMSE	5.50	1.36	4.83
Longs Creek			
n	13	13	12
R ²	0.939	0.940	0.827
P-score	<0.001*	<0.001*	<0.001*
Bias	-5.69	-0.773	-0.884
RMSE	5.85	1.67	4.68
Mactaquac Causeway			
n	14	14	13
R ²	0.949	0.945	0.845
P-score	<0.001*	<0.001*	<0.001*
Bias	-6.30	-1.48	-1.68
RMSE	6.47	2.29	4.83
Combined Below Dam			
n	40	40	38
R ²	0.948	0.956	0.837
P-score	<0.001*	<0.001*	<0.001*
Bias	-5.82	-0.990	-1.01
RMSE	5.96	1.82	4.78
Combined above dam			
n	19	19	11
R ²	0.864	0.872	0.150
P-score	<0.001*	<0.001*	0.239
Bias	-3.77	1.08	-3.55
RMSE	4.19	2.42	7.15

* Indicates significance at alpha value of 0.05

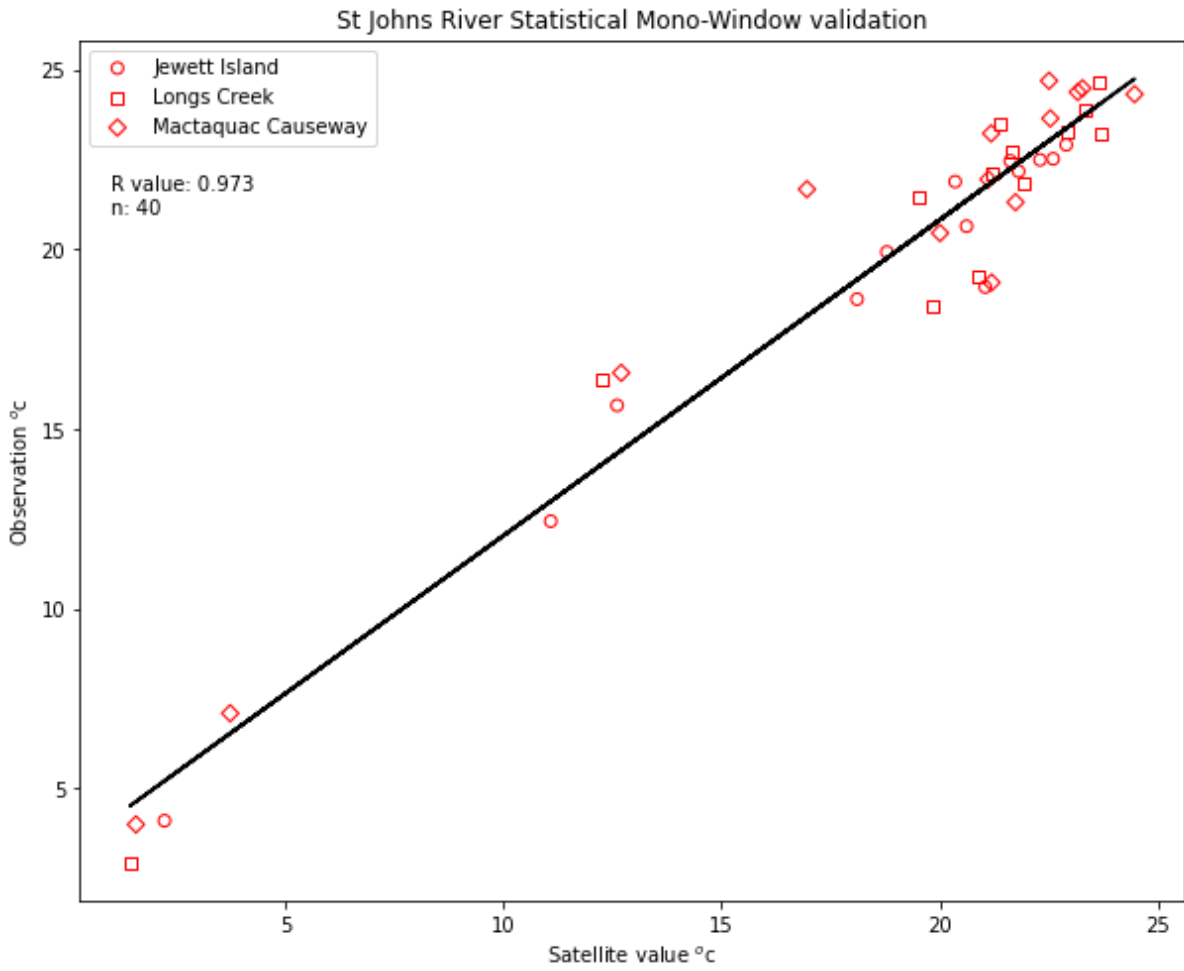


Figure 9: Comparison between satellite and in-situ logger river temperature values downstream of the Mactaquac Dam on the St John's River. Markers used to visual different logger locations, using the Statistical Mono-Window method with the 'BQA' band cloud algorithm.

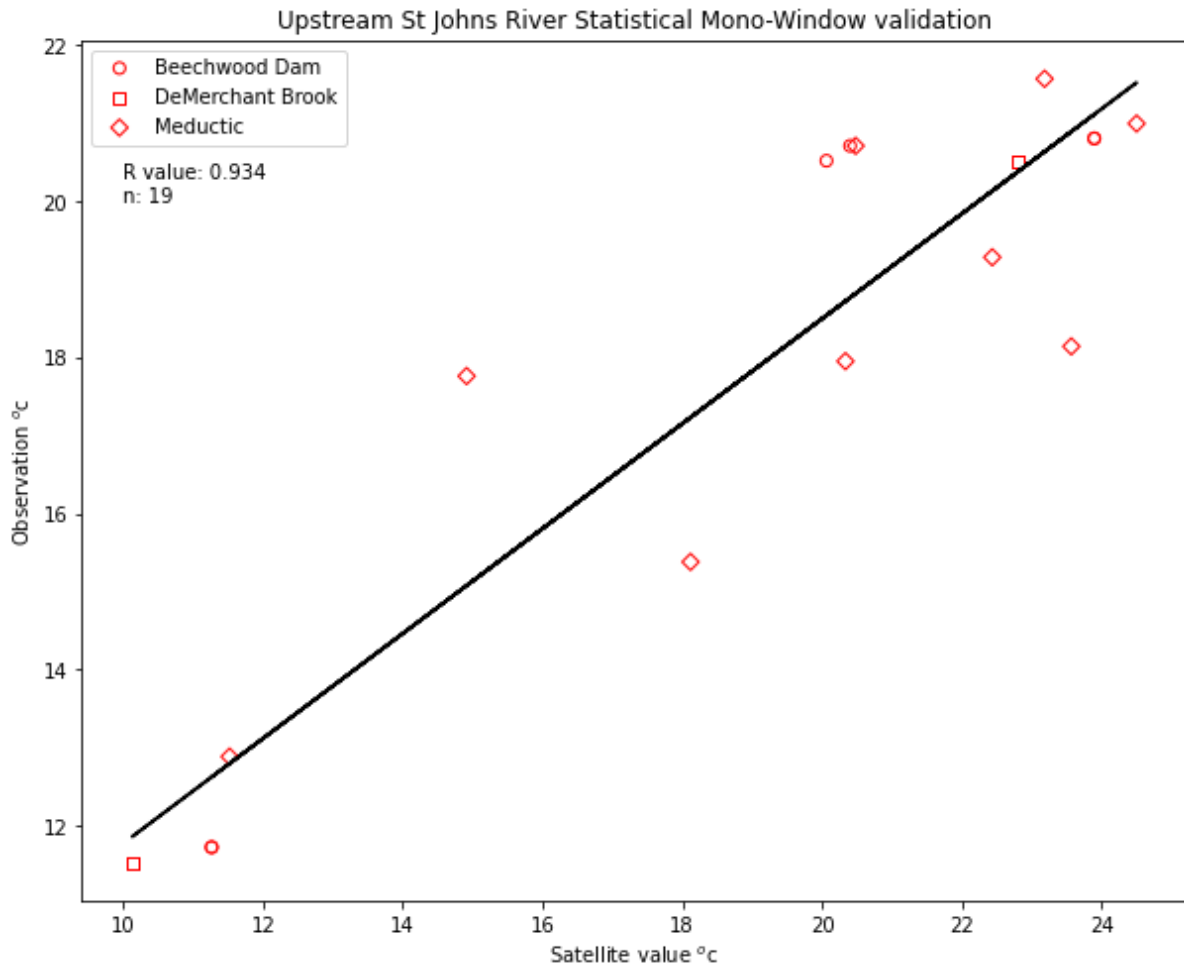


Figure 10: Satellite and sensor comparison upstream of the Mactaquac Dam on the St John's River. Markers used to visual different logger locations. These loggers are at deeper locations so display the impact of only measuring the water surface on the ability of the method to represent water temperature.

5.4.2 Colorado River, Arizona, USA

The method was not able to be successfully validated at all sites. At some sites this is because the channel has moved and instead, values are returned from in-channel bars (Figure. 8). In others when matching against logger data the results were weaker than other sites. The Colorado river below Glen Canyon dam produced visualisations that on the surface looked like the accurate images produced at other sites (Figure. 11). Pearson's R^2 values of 0.287 ($p < 0.001$, $n = 134$) highlighted a much weaker correlation between the values recorded by the temperature loggers and satellite observations (Figure. 12). Site 9404200 produced the highest correlation of all loggers in this section of the Colorado with a RMSE of 13.1°C with a bias of 8.32°C, all other logger results are available in Appendix B. Further, this indicates that the GEE method may not always be applicable to all rivers and requires further investigation.

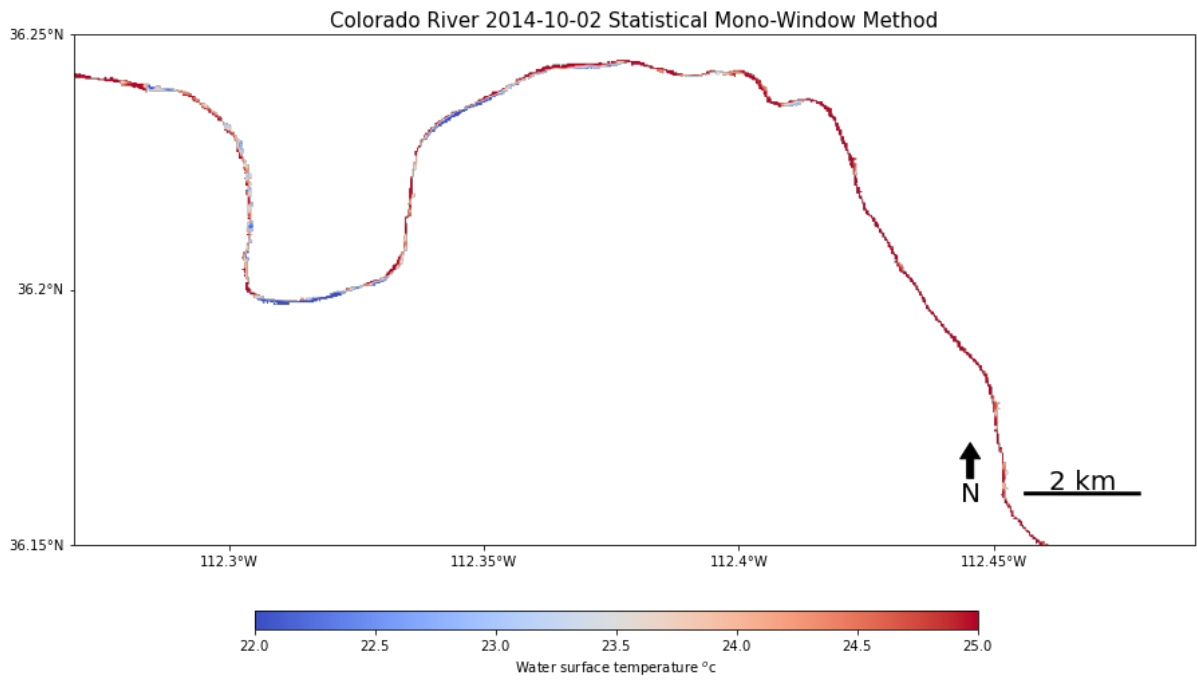


Figure 11: Colorado River using SMW river temperature method. Without comparing these values to actual river temperature, it would appear this image is similar to Figure. X.5.1 but in fact this represents an erroneous record of temperature 10°C warmer than observed at the site.

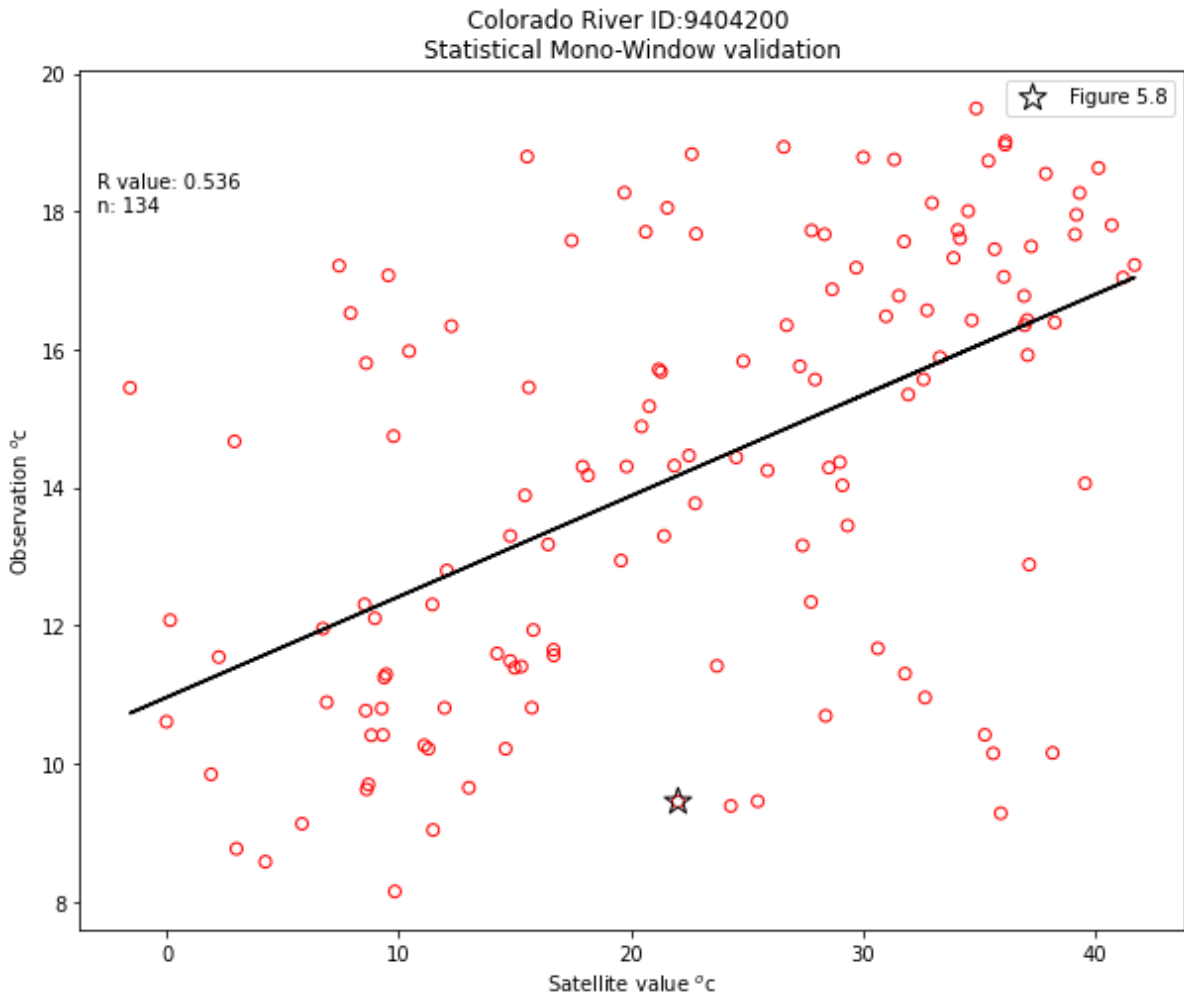


Figure 12: Lack of correlation between satellite surface water temperature and in-situ loggers in at the Colorado River below Glen Canyon. Note the increase in points is due to extended period of validation data available and the relative lack of cloud at this site.

5.6 Atmospheric Correction

The three atmospheric correction methods produced similar results (Table. 4) but the correlation coefficients were found to exhibit significant differences the PSC and other methods (Table. 5) using the Fisher-Z Transformation. The SMW method produced the highest Pearson's correlation which was found to be significantly better than the PSC method. It also produced much lower values for RMSE and Bias which may separate it from the NAC method despite the correlations not being significantly different (Figure. 13). The PSC method also copped worse with the 3 upstream loggers on the Saint John River, which were set deeper in the water column, and produced much poorer RMSE (Table. 4).

Table 5: Comparison between the different methods, using the 2-tailed Fisher-Z transformation, found significant difference between the Non-Atmospherically Corrected (NAC) method and the Practical Single Chanel (PSC) methods. As well as significant difference between the Statistical Mono-Window (SMW) and the PSC method. This used 3 downstream loggers on the St John's River between 2014 and 2015.

Comparison	Z-score	P-score
NAC-SMW	-0.37	0.711
NAC-PSC	2.55	0.011*
SMW-PSC	2.91	0.004*

* Considered significant at the 0.05 Alpha level set

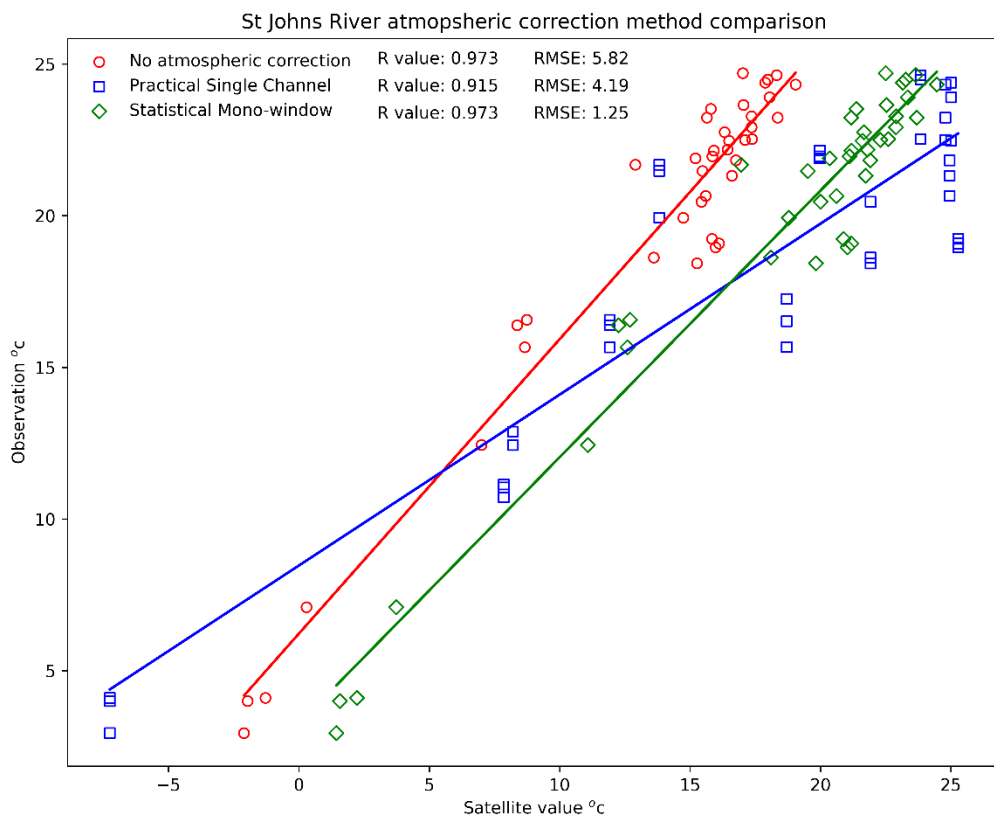


Figure 13: A comparison displaying the different results obtained using different atmospheric correction methods. The methods can be altered to account for the bias they are currently showing but the error and scatter is harder to improve upon.

6.0 Discussion

As the results have shown, all three objectives were met. An assessment was made of the ability of GEE to enhance the speed and usability of satellite TIR river temperature, by using rapid visualisation tools to disseminate results. Some misgivings about relying on GEE were unearthed and are discussed here. Results were validated in a number of different scenarios which proved the method worked, but care needs to be taken because the tool was found not to be universally transferable. Suggestions are presented on how these erroneous catchments can be managed and where improvements in accuracy can be made. Using the structure built by the first two objectives, the Statistical Mono-Window (SMW) atmospheric correction method was found to be more accurate than the Practical Single-Channel (PSC) method or analysis with no atmospheric correction (NAC), and the causes for this are discussed.

6.1 Potential and limitations of GEE

It is clear from the results that the potential of GEE meets many of the claims made for increasing the ease with which difficult computing tasks can be managed (Gorelick et al., 2017). It provides a powerful tool to carry out the computationally expensive task of converting TIR data and atmospheric data from multiple sources into a river surface temperature without needing to download or store any hard drive data (Bonnema et al., 2020).

Before the limitations that have been noticed here are presented, it should be acknowledged that the tool is still in relative infancy. Less than a decade ago the images used in this study were proprietary data, therefore, to be able to calculate and analyse hundreds of images on a standard laptop is a significant development over previous methods. This is especially true of the app created (Valman, 2021a) which if carefully managed could provide a useful tool for rapid interactive river temperature assessment without the requirement for knowledge of remote sensing or programming.

However, it is precisely this proposed ability to reduce the need for advanced remote sensing knowledge that has provided the most misgivings in this study. GEE creates a 'black box' (Loyola-Gonzalez, 2019) computing environment where much of the calculations are carried out server side. This can leave many of the key assumptions of methods missing. One example of this is the difficulty in scrolling through images to check that the georeferencing is

exact enough to be extracting and comparing the same pixel in every attempt. To scroll through images requires conversion to a list and then converting each item back to an image and plotting them to a map individually. If the user does not have a good knowledge of the mixed-pixel problem (Kale et al., 2017) or contextual knowledge of channel change (Boothroyd et al., 2021) then this can lead to erroneous results which are acted upon without knowledge.

Similarly, the flip side of GEE encouraging speed of visualisation is that it makes it very difficult to extract temperature values and general statistics. Processing and resampling are not carried out until the user “calls” for it, either by zooming in the visualisation or by extracting a point (Navarro, 2017). This means that it is not easy to extract max or minimum points from a scene. Often these statistics meet the MaxPixel Error which limits the number of pixels that can be extracted to protect the GEE servers from being overloaded, and causes the coding script to fail (GEE, 2021d). It also limits the ability to extract entire scenes of GEE and check their georeferencing in traditional GIS software, therefore only sections can be compared to images directly downloaded from the USGS (USGS, 2021a). This means that the pre-processing carried out by GEE had to be trusted.

Moreover, extracting data points is much more time consuming than visualising the data. This is because of the server-side cloud computing nature of the method which does not carry out any computations or resampling until called to do so. This “call” happens when the user either scrolls in to get a closer view on a map or when they interrogate a cell for a value. While these are not significant drawbacks and are integral to the speed and power of GEE, they require the user to have more knowledge of remote sensing than might otherwise be assumed by the friendly nature of the method and the ease of using freely available scripts made by researchers.

This need to trust GEE extends to much of the documentation and many of the algorithms which are built into GEE (GEE, 2021e). For example, unsuccessful attempts to reduce the required computations and implement the radiative transfer equation technique met the simple risk of not checking secondary metadata on the GEE catalogue (GEE, 2021b) against the original Landsat metadata (USGS, 2020). The band rescaling factor for the transmissibility band was out by an order of magnitude, which was fixed after I alerted GEE developers (Ilyushchenko, 2021). However, without bringing this to the attention of developers it is difficult to know if it is a metadata error or a difference between the original data and that provided by GEE.

This is the case with the ToA algorithm which was applied in some of the cases here. The algorithm was only required by the non-atmospherically corrected method as both the PSC and SMW methods used pre-processed ToA data. The calculation was re-written here

because the GEE version did not include the -0.31 correction constant defined in the literature (Chander et al., 2009, Avdan and Jovanovska, 2016). Again, this is another example, of the black box nature of GEE as the correction factor is also not included in the pre-processed ToA product. It was decided that the PSC and SMW methods would not be altered in this case so that each algorithm matched its original source.

6.1.2 The *SatTemp* Python Package

Despite the limitations presented above, the package developed here (Valman, 2021b) can provide significant time and knowledge short cuts to enable dam operators to obtain river temperature data for their own sites. It is downloadable through PiP (instructions in repository) and therefore can be used with whichever version of the Python API is desired, such as Jupyter Notebooks, Qpy, or traditional Python interpreters. With the correct metadata to understand the choices that are being made and the equations being used in this package it allows a researcher to simply plug in the dates and geometry of their chosen study site and collect results that they are able to test for accuracy and start work on.

The package detaches users further from the programming decisions made but calculations are written as text-string GEE expressions to ease transparency. The package is downloaded from an open-source GitHub repository meaning these calculations can be seen and commented on, consequently if later versions contain typing errors these can be picked up on by the user and changes requested as opposed to guessing the contents of GEE algorithms.

As will be discussed, some of the limitations of the study will be built into future package versions including more options for cloud cover analysis, channel centreline prediction, river water mask options, and longitudinal graph options.

6.1.3 Enhanced dissemination: “*RiverTemperatureApp*”

The app developed here, named “*RiverTemperatureApp*” (Valman, 2021a), is the most contentious part of the project because it incorporates all the limitations which have been presented here. It allows the user to select the date and area, and then produce visualisations of river temperature without the need to validate these or the ability to see the code beneath. However, should this be made proprietary it would be a useful tool for those with the knowledge to customise outputs where it is known to work. This would produce a dashboard of important findings for operators to use which could be pre-checked by an expert to make

sure it works in that context. The widgets used could also be constrained to fit its area of use, for example building regular longitudinal plots which compare river temperature to past temperatures at a similar time of year. These longitudinal plots would be especially important to enable dam operators to co-ordinate releases where multiple large dams exist in a sequence (Skalak et al., 2013) and temperature effects from each can last up to 260km downstream (Xiong et al., 2020). All these factors suggest that as a working concept the app is successful but due to the limitations and difficulties within the data it should be rolled out very carefully only to sites it where some form of validation and contextual knowledge is available.

6.1.4 Automation or application of community datasets

While many of the limitations with using GEE in a project like this are universal and can be applied to other time stacked cloud computed dissemination studies, the large rivers on which hydropower and large industry operate create some specific problems that need accounting for.

As argued in the literature review, river temperature can change over diurnal cycles but a 16-day return period from Landsat data is sufficient to obtain readings appropriate for dam operations. It was found that images at the same site usually occurred within a 5-minute window of the same time of the day each pass over (appendix A), so the temporal aspect was relatively well controlled. To accurately judge the impact that dams are having would require some form of release schedule so that river temperature readings could reflect how much water is being released. For the same reason, air temperature should also be included in river temperature readings to enable investigation of whether changes in river temperature are climatic or anthropogenic in nature.

Another way to increase the usability of results would be to include ASTER which has a similar return period thus doubling the available data during the Landsat 8 Recording interval (Despini and Teggi, 2013). This would make it more feasible to compare temporally as there would be more likelihood of having results from the same month in previous years to compare to. ASTER TIR data is usually analysed using a split-window algorithm due having multiple thermal bands. Therefore, any combination of the different satellites would require an understanding of the different errors caused by having two different algorithms.

The Global River Width from Landsat (GRWL; Allen and Pavelsky, 2018) has been shown to be very useful in helping to delineate and visualise the results here. These global datasets do

have some problems in the context of highly dynamic river systems. Channel change occurs in single storms and floods which can occur between monitoring periods, thus especially with channel avulsion the channel can rapidly no longer represent the GRWL map provided. It is suggested that future studies should include the raw algorithms (Allen and Pavelsky, 2018, Yang et al., 2019, Boothroyd et al., 2021) in order to extract the river shape from each Landsat image used. This may create continuity issues for comparing rivers globally but for the context of dam operators, single points of time would usually be visualised rather than mean values.

The importance of automated channel feature extraction is greater for the extraction of data values to graphs and results. By recalculating river width with each image, an error would be thrown if a logger point was no longer a clear pixel which would help manage the possibility of mixed pixels. The mixed-pixel issue would also be managed in longitudinal diagrams where in channel bars were likely to be the cause of errors in the River Ganges (Figure. 8) 2017 and 2018 results. This is because the channel was likely to have moved since the original centreline was drawn in 2015 and is expected to be the cause of the error. This is especially important in the study of dams which have the ability to flush sediment, maintaining downstream supply and preventing the reservoir from silting up, which can rapidly impact downstream morphology (Fruchard and Camenen, 2012). This can impact a river very easily between two records, especially if suggestions to coincide sediment releases with flood peaks (Dahal et al., 2021) are met. Thus, it is important to recalculate channel centreline with each image rather than rely on global products that may be updated annually or less. While this is more important in a study of this kind, the premise is likely to be true for many of the major datasets on landcover or habitat (Roy, 2020) type which can quickly become outdated, and it is recommended that best practise is to provide the algorithm in an easy-to-use format so results can be revaluated with successive studies rather than a dataset which needs constant updating and version control.

6.2. Relationships between in-situ kinetic loggers and satellite TIR

Objective 2 required that the study was validated in a number of streams to assess how accurate the method was at matching real-world data. In doing so, it has been shown that the method produces accurate results in two large rivers with very different climates (the Saint John River and the Ganges) and one case study where it does not work (the Colorado River). Arguably, it has been useful to have a river where the method is not appropriate because it gives some idea of the limitations of the method.

6.2.1. Validation statistics

Three main validation factors were used: Pearson's R^2 , RMSE and bias. To meet the objective set out, R^2 and RMSE were considered more important because they assess method accuracy whereas users can simply include a constant to counteract a known bias. For example, the SMW method produced bias levels in the three downstream river reaches that were similar with a range of just 0.8°C suggesting this might be a constant underestimation. In this context it would be useful to obtain water temperature logger results from other large streams to assess if the bias is impacted by different climate zones. To some extent, the Ganges longitudinal plots (Figure. 8) can be used for this because the general trend is towards values 1.5°C lower than the Yadav et al. (2020) study. Regardless, values from temperature loggers would be preferable, even with the expense of field surveys, to provide empirical comparable results.

If bias is consistent, R^2 and RMSE can tell us how accurate the method is at predicting river surface temperature because it shows how likely it is to under or over predict temperature. In the Saint John River, a highly significant ($n=40$, $p<0.001$, $\alpha=0.05$), strong correlation of 0.96 was found. This is similar to other studies which found R^2 correlations of 0.92 (Bonnema et al., 2020). Moreover, the RMSE of 1.82°C was only slightly higher than studies with similar river widths (Martí-Cardona et al., 2019) but lower than land surface temperature studies carried out without atmospheric correction (Avdan and Jovanovska, 2016). When compared to airborne remote sensing, which can have an RMSE of $\sim 0.5^\circ\text{C}$ (Dole-Olivier et al., 2019), the results are very good considering the almost complete reduction in costs of applying this method in comparison to flying an aerial survey.

Despite positive results, it is important to understand what might be driving error in satellite-derived values, indications of which may be found in the upstream loggers ($n= 19$, R^2 : 0.87, $p<0.001$, RMSE: 2.42°C). The loggers in this upstream cluster are lower in the water column and so are providing kinetic temperature that is impacted by thermal stratification at depth, even if, as this literature claims, this does not have a large impact on results (Talke et al., 2013) it will have some impact. In a similar way, many of the other studies are not assessing the success of their methods in a standardised manner. All TIR satellite methods measure stream radiant temperature, the exchange of heat from a surface, therefore this is likely to differ from the kinetic water temperature that temperature loggers measure (Jensen et al., 2014). Other studies use local air temperature to assess their results which may account for their lower accuracy (Avdan and Jovanovska, 2016) or use hand-held spectrometers which also record radiant water surface temperature and therefore are more similar to satellite values (Martí-Cardona et al., 2019). This means that any comparison between studies should be

aware of these possible discrepancies. It is important to remember that kinetic temperature is the variable that directly relates to dam operation, fish stocks, and algal blooms. Therefore, the error in predicting this variable is the salient information to collect for engineers and managers to justify decisions based on satellite TIR.

Stream temperature models can produce similar RMSE and once produced can be used with similar lack of cost (Piotrowski et al., 2021). However, they still rely on meteorological point data which makes their effectiveness in different systems and in the context of anthropogenic alterations hard to manage (Dugdale et al., 2017). As such, temperature models trained on satellite derived river temperature can be produced from results such as those found here (Tavares et al., 2020). These assimilation models may take both the benefits of accurate, regular temperature prediction and continuously updated satellite images to detect changes within the system and its operation.

6.2.2. Sources of error unique to the Colorado River

The method was shown to not work on the Colorado River, Arizona USA. This can help us collect a list of scenarios where the method may not work which can be tested in future studies. The first and most likely reason is the impact of mixed pixels on the results due to this river being considerably less wide than the other two in the study with logger sites ranging from 200m to 85m (as opposed to 840m to 330m in the Saint John River). However, even without the pixel-unmixing strategies presented (Martí-Cardona et al., 2019) the wider sections of this river should have been wide enough to meet the upper estimates required for satellite TIR river temperature monitoring, which suggest river widths of at least 180m (Handcock et al., 2006).

Therefore, further research should look into the other possible causes of the weaker correlation and higher RMSE found on the Colorado River. The logger types are similar to those used on the Saint John River, so it is unlikely to be a measurement artifact caused by the loggers. Turbulent “whitewater” has been shown to be capable of significantly altering emissivity values (Talke et al., 2013) and while there are considerable examples of this in the Grand Canyon, none of the logger sites exhibit this. Moreover, in future studies it is worth noting that these turbulent sections are more likely to occur at narrow points in the channel rather than wide points and therefore smaller river reaches may be avoided for temperature extraction regardless.

The main two factors beyond width which separate the Colorado from other rivers in this study is the increased temperature difference between night and day (Voichick and Wright, 2007). There has been a lack of research into the speed with which this may impact temperature in the water column, and how quickly the measured radiant water surface temperature may increase in comparison. The other factor that could be the cause or contribute to the large error in results is the fact that this in geomorphological terms this is a valley confined river (Brierley and Fryirs, 2013). In terms of engineering this makes it a good place to build a dam because the valley walls can anchor the structure (Bruce, 2005) however it is proposed that these same valley walls may create effects similar to that of cloud shadow and thus disrupt the emitted radiation recorded. It is also proposed that these valleys could confine concentrations of air-water vapour which are not accounted for by atmospheric correction. This should be tested for in future studies because it would have substantial implications for current projects for dams as well as implications for future higher resolution satellite remote sensing (Mo et al., 2018) for other uses including urban heat effects (Ali et al., 2017).

6.3 Strategies for increasing accuracy

A RMSE score below 2°C is positive but there are some areas in which it could be improved. The integration of more advanced cloud masking techniques and automated channel design is one way of reducing outlying results. Moreover, the improvement of pixel quality and resolution through the introduction of pixel unmixing strategies (Martí-Cardona et al., 2019) and sharpening water algorithms (Despini and Teggi, 2013) should be investigated for their ability to improve RMSE, especially in thinner river channels.

Emissivity may also play a role in reducing the RMSE of the results. Emissivity is taken as a constant here and the possible alternative values used in the literature are very similar to those used here (e.g., Lamaro et al., 2013) and are therefore unlikely to create large error differences. Especially, as the value here matched the value used for the most accurate satellite TIR river temperature paper discussed (Martí-Cardona et al., 2019). Therefore, to significantly improve the emissivity part of the calculation it may be appropriate to test a fluctuating emissivity value based on suspended sediment approximated by the river water colour (Gardner et al., 2021) or by feature extraction floating vegetation and different surface water dynamics (Handcock et al., 2012).

6.3.1 Cloud cover improvements

The cloud cover algorithm applied here was one of the simplest options relying on the analysis already carried out by Landsat (Foga et al., 2017). This was also the method originally used in the SMW algorithm when it was first developed by Ermida et al. (2020). It was considered reasonably successful for the task at hand, especially where cloud creates noticeably extreme negative temperature readings alerting the user to errors (Bonnema et al., 2020). However, it was found that cirrus cloud was harder to detect and may have been part of the cause for some erroneous points on the Colorado River. These errors only accounted for a few points and therefore cannot have been the sole cause of the weak correlation found using the Colorado River (Figure. 12). Still the best way to manage cloud is to open a RGB optical satellite image and manually look for it (Zhu and Woodcock, 2012). Again, if these methods had been carried out in traditional GIS software images would have been visualised upon downloading, making it possible to notice where cloud had not been appropriately retracted but the GEE method does not provide these visual processing steps unless manually implemented. In future studies, more advanced cloud cover algorithms should be employed to maintain the benefits of cloud computing but improve cloud cover removal (Hollstein et al., 2016).

6.4. Extending river temperature extraction to more rivers

The majority of values returned from the Colorado river are between 10 and 20 degrees Celsius and therefore without validation or expected temperature intervals created from air temperature models (Mohseni et al., 1998) an unskilled practitioner using my app could make assumptions based on these results. If future work on the project enables users to transfer the method anywhere then it should include some form of confidence bounds.

Error brackets, defining the likelihood of a remotely sensed water temperature value being correct based on modelling expected water temperature from air temperature, would help identify river systems that are not compatible with this satellite river temperature measurement method. Validating the results in each new river system would provide more assurance that it is a viable system to monitor through satellite remote sensing. This would also allow dam operators an estimate of the error and bias in the results which they can act upon. The results from the Saint John River show that a two-year interval with a limited number of loggers is appropriate to provide this validation. With temperature loggers becoming more affordable, with a 1-year battery life it may be appropriate to carry out validation in more sites and

thereafter rely on satellite remote sensing. Aerial and UAV TIR remote sensing methods may also be viable methods for creating validation data especially where other studies are also occurring, however this would be a comparison between two sources of radiant river water temperature and therefore the issues highlighted earlier will still need to be addressed here.

6.5 Atmospheric correction and potential

Testing the different atmospheric correction algorithms resulted in finding the SMW method to be the most effective method used in this study. This is interesting because the PSC method had otherwise been proven to be more effective at matching near ground temperature values in a direct comparison between the two methods (Wang et al., 2020b).

What is perhaps more interesting is that the method with NAC produced relatively good results. Applying a method without atmospheric correction to a water context has been shown to be reasonable with on clear days of no humidity but to produce increasing errors as air water moisture content increases (Wang and De Liberty, 2005). The ability of the method to provide a strong correlation could be attributed to the high emissivity value chosen, by being so close to a black body object its almost perfect emittance makes the atmosphere a smaller but not entirely negligible factor. Thus, in some cases the methods correct for this atmospheric interference but in others, due to the high emissivity value they can overcorrect. The NAC RMSE value around 5°C reduces the usability of this data but it does allow the quantification of the improvement or overestimates provided by the atmospheric correction algorithms. In this case the SMW may reduce the error by nearly 4°C, whilst the PSC only reduces error by 1°C.

Bias results from this study differ from similar studies (Martí-Cardona et al., 2019) in that they do not show an overprediction of temperature expected from Landsat sensors (Barsi et al., 2014). The cause of this may be the radiative transfer equation and model applied in other studies (e.g., Zhao et al., 2020), When an approximation of values were built based on a linear version of this radiative transfer model for the SMW method (Ermida et al., 2020), it is possible the overcorrection from this model was accounted for. To test this, the recently released Landsat Collection 2 product which relies on a similar but different model to produce upwelling radiance, downwelling radiance and transmissibility (USGS, 2020) should be built into a GEE radiative transfer equation method to test against those presented here. Should this prove a better algorithm it could be entered into the SatTemp package as another option.

Increasing the atmospheric correction methods in the package and testing these against those presented here would help continuously improve temperature monitoring. Some of the most effective methods are not yet available on GEE (Meng and Cheng, 2018) but with ever increasing data availability the accuracy of these methods may still be improvable.

7.0 Conclusion

The research has aimed to discover to what extent GEE is a viable tool for the extraction of river temperature, to be used in dam operating procedures, globally. It has been shown that GEE is capable of rapidly calculating river temperature from a collection of time stacked Landsat 8 images. I have displayed the ability Python API to generate packages of functions (Valman, 2021b) which reduce the time taken for operators to apply these methods. GEE has also been used to create an interactive app (Valman, 2021a) for users to apply these methods without needing programming knowledge. However, it is felt that the black box nature of GEE, and the products delivered here, necessitate more research into the appropriate ways in which these findings are disseminated, in order to reduce the risk of misleading users who are not privy to all the decisions and appropriate error statistics in these methods.

Meeting objective two has shown that the method is capable accurately monitoring river temperature, as it did in the Saint Johns River. Accuracy was found to be within 2°C which is considered very successful for measuring kinetic river temperature. Comparisons with other sites and studies need to account for how validation data is collected, be it the depth of logger or the method of collection. The paucity of available in-situ temperature readings made it difficult to test the transferability of the method. It is clear that in some cases, such as the Colorado River, the method is not yet appropriate. This may be because of the climate, high walled valley-confined stream type, or narrow river channel width. Further research is required to detect which cause is responsible and if these causes are site specific to the Colorado River or universal rules that should be applied to all river satellite TIR sensing. For now, it is recommended that the method is not used without at least 2 years validation data as shown on the Saint Johns River.

The third objective was to assess the need for an atmospheric correction technique in this context and compare this against the Statistical-Mono Window and Practical Single-Channel methods. It was found that results were producible without atmospheric correction, but the most accurate method was to correct for atmospheric effects using the SMW algorithm. This

algorithm reduced RMSE by nearly 4°C. Clear assessment of how well the different methods work in different biomes would require the availability of more validation data from which to find correlation, bias and RMSE values. In the wider literature it appears that there are other more successful atmospheric correction factors which require datasets which are not currently available on GEE (Meng and Cheng, 2018, GEE, 2021b). Future research should aim to include these in the SatTemp package as soon as they are available and compare them to current methods to enable a continuous maximisation of monitoring accuracy.

The project has created multiple exciting avenues for future research to produce dam operational benefits. The results can be extended temporally because the SMW method is also compatible with Landsat 4, 5 and 7, meaning trends in river temperature change could be used for regulators to govern rules of cold water dam releases. For dam operators increasing the current temporal resolution would enable more regular outputs with which to populate the dashboard. This could be achieved through inclusion of ASTER TIR sensors or building assimilative models trained on this satellite data. At the moment the method presented here still requires personnel with contextual knowledge of the river system in question, and some background in remote sensing to acknowledge the decision made in these processes.

Regardless of the direction that future research takes, it has been demonstrated that it is possible for GEE and Landsat 8 to produce river temperature measurements and be used as a tool to increase the speed of dissemination of these results. To the best of my knowledge, this is the first study to compare atmospheric correction techniques solely in river systems, with the goal of providing actionable insight. It is also the first to build a package that can seamlessly transition between atmospheric correction methods using the same input data by selecting the method from a list. This has built a foundation for further automated algorithms to be built in to improve the accuracy of the method and create meaningful dashboard insights such as automated longitudinal profiles which can be added to the app to manage water releases.

8.0 Reference List

- Abolt, C., Caldwell, T., Wolaver, B. & Pai, H. 2018. Unmanned aerial vehicle-based monitoring of groundwater inputs to surface waters using an economical thermal infrared camera. *Optical engineering*, 57, 053113.
- Abrams, M., Hook, S. AND Ramachandran, B. . 1999. *ASTER Users Handbook* [Online]. Available: https://lpdaac.usgs.gov/documents/262/ASTER_User_Handbook_v2.pdf [Accessed 13th August 2021].
- Ahlers, R. 2020. Where walls of power meet the wall of money: Hydropower in the age of financialization. *Sustainable Development*, 28, 405-412.
- Ahmad, S. K. & Hossain, F. 2020. Realizing ecosystem-safe hydropower from dams. *Renewables: wind, water, and solar*, 7, 1-23.
- Al-Murib, M. D., Wells, S. A. & Talke, S. A. 2019. Integrating Landsat TM/ETM+ and Numerical Modeling to Estimate Water Temperature in the Tigris River under Future Climate and Management Scenarios. *Water*, 11, 892.
- Alashhab, Z. R., Anbar, M., Singh, M. M., Leau, Y.-B., Al-Sai, Z. A. & Alhayja'a, S. A. 2021. Impact of coronavirus pandemic crisis on technologies and cloud computing applications. *Journal of Electronic Science and Technology*, 19, 100059.
- Ali, J. M., Marsh, S. H. & Smith, M. J. 2017. A comparison between London and Baghdad surface urban heat islands and possible engineering mitigation solutions. *Sustainable Cities and Society*, 29, 159-168.
- Allen, G. H. & Pavelsky, T. M. 2018. Global extent of rivers and streams. *Science*, 361, 585-588.
- Arismendi, I., Safeeq, M., Dunham, J. B. & Johnson, S. L. 2014. Can air temperature be used to project influences of climate change on stream temperature? *Environmental Research Letters*, 9, 084015.
- Armitage, R. P., Alberto Ramirez, F., Mark Danson, F. & Ogunbadewa, E. Y. 2013. Probability of cloud-free observation conditions across Great Britain estimated using MODIS cloud mask. *Remote sensing letters*, 4, 427-435.
- Avdan, U. & Jovanovska, G. 2016. Algorithm for Automated Mapping of Land Surface Temperature Using LANDSAT 8 Satellite Data. *Journal of Sensors*, 2016, 1480307.
- Barsi, J. A., Barker, J. L. & Schott, J. R. An atmospheric correction parameter calculator for a single thermal band earth-sensing instrument. IGARSS 2003. 2003 IEEE International Geoscience and Remote Sensing Symposium. Proceedings (IEEE Cat. No. 03CH37477), 2003. IEEE, 3014-3016.
- Barsi, J. A., Schott, J. R., Hook, S. J., Raqueno, N. G., Markham, B. L. & Radocinski, R. G. 2014. Landsat-8 Thermal Infrared Sensor (TIRS) Vicarious Radiometric Calibration. *Remote Sensing*, 6, 11607-11626.
- Bloom, A. & Novacheck, J. 2017. The Eastern Renewable Generation Integration Study: Insights on System Stress. National Renewable Energy Lab.(NREL), Golden, CO (United States).
- Board, O. S., National Academies Of Sciences Engineering & Medicine 2019. *Environmental engineering for the 21st century: Addressing grand challenges*, National Academies Press.
- Boelens, R., Shah, E. & Bruins, B. 2019. Contested knowledges: Large dams and mega-hydraulic development. Multidisciplinary Digital Publishing Institute.
- Bonnema, M., Hossain, F., Nijssen, B. & Holtgrieve, G. 2020. Hydropower's hidden transformation of rivers in the Mekong. *Environmental research letters*, 15, 044017.

- Boothroyd, R. J., Williams, R. D., Hoey, T. B., Barrett, B. & Prasojo, O. A. 2021. Applications of Google Earth Engine in fluvial geomorphology for detecting river channel change. *Wiley Interdisciplinary Reviews: Water*, 8, e21496.
- Boyer, C., St-Hilaire, A., Bergeron, N., Daigle, A., Curry, R., Caissie, D. & Gillis, C. 2016. RivTemp: a water temperature network for Atlantic salmon rivers in eastern Canada. *Water News*, 35.
- Brierley, G. J. & Fryirs, K. A. 2013. *Geomorphology and river management: applications of the river styles framework*, John Wiley & Sons.
- Bruce, D. A. Evolution of rock anchor practice over three decades. Proc., Ann. Geotech. Eng. Conf., Minnesota Geotechnical Society, St. Paul, MN, 2005.
- Caissie, D. & El-Jabi, N. 2020. The importance of cross-calibration and protecting water temperature sensors against direct solar radiation heating in hydrological studies. *Hydrological Sciences Journal*, 65, 102-111.
- Cha, Y., Cho, K. H., Lee, H., Kang, T. & Kim, J. H. 2017. The relative importance of water temperature and residence time in predicting cyanobacteria abundance in regulated rivers. *Water research*, 124, 11-19.
- Chander, G., Markham, B. L. & Helder, D. L. 2009. Summary of current radiometric calibration coefficients for Landsat MSS, TM, ETM+, and EO-1 ALI sensors. *Remote Sensing of Environment*, 113, 893-903.
- Chapra, S. C., Boehlert, B., Fant, C., Bierman JR, V. J., Henderson, J., Mills, D., Mas, D. M., Rennels, L., Jantarasami, L. & Martinich, J. 2017. Climate change impacts on harmful algal blooms in US freshwaters: a screening-level assessment. *Environmental Science & Technology*, 51, 8933-8943.
- Chen, J., Shi, H., Sivakumar, B. & Peart, M. R. 2016. Population, water, food, energy and dams. *Renewable and Sustainable Energy Reviews*, 56, 18-28.
- Choi, D. H., Park, J. S., Hwang, C. Y., Huh, S. H. & Cho, B. C. 2002. Effects of thermal effluents from a power station on bacteria and heterotrophic nanoflagellates in coastal waters. *Marine Ecology Progress Series*, 229, 1-10.
- Dahal, S., Crosato, A., Omer, A. Y. & Lee, A. A. 2021. Validation of Model-Based Optimization of Reservoir Sediment Releases by Dam Removal. *Journal of Water Resources Planning and Management*, 147, 04021033.
- Daigle, A., Caudron, A., Vigier, L. & Pella, H. 2017. Optimization methodology for a river temperature monitoring network for the characterization of fish thermal habitat. *Hydrological Sciences Journal*, 62, 483-497.
- Daniels, M. E. & Danner, E. M. 2020. The Drivers of River Temperatures Below a Large Dam. *Water Resources Research*, 56, e2019WR026751.
- Danielsson, P., Postema, T. & Munir, H. 2021. Heroku-Based Innovative Platform for Web-Based Deployment in Product Development at Axis. *IEEE Access*, 9, 10805-10819.
- Dauwalter, D. C., Fesenmyer, K. A., Bjork, R., Leasure, D. R. & Wenger, S. J. 2017. Satellite and airborne remote sensing applications for freshwater fisheries. *Fisheries*, 42, 526-537.
- Despini, F. & Teggi, S. 2013. Analysis of temperature maps of waterbodies obtained from ASTER TIR images. *International Journal of Remote Sensing*, 34, 3636-3653.
- Díaz, C. P., Xiong, X. & Wu, A. MODIS thermal emissive bands calibration stability using in-situ ocean targets and remotely-sensed SST retrievals provided by the group for high resolution sea surface temperature. Ocean Sensing and Monitoring XI, 2019. International Society for Optics and Photonics, 110140P.
- Dole-Olivier, M.-J., Wawzyniak, V., Des Chatelliers, M. C. & Marmonier, P. 2019. Do thermal infrared (TIR) remote sensing and direct hyporheic measurements (DHM) similarly detect river-groundwater exchanges? Study along a 40 km-section of the Ain River (France). *Science of the Total Environment*, 646, 1097-1110.
- Donchyts, G., Baart, F., Winsemius, H., Gorelick, N., Kwadijk, J. & Van De Giesen, N. 2016. Earth's surface water change over the past 30 years. *Nature Climate Change*, 6, 810-813.

- Dufour, F., Tatin, M., Simon, A., Briffaut, M. & Fabre, J.-P. Thermal displacements of concrete dams: accounting for water temperature profile in statistical model. 2nd Int. Dam World Conf, 2015.
- Dugdale, S. J. 2016. A practitioner's guide to thermal infrared remote sensing of rivers and streams: recent advances, precautions and considerations. *Wiley Interdisciplinary Reviews: Water*, 3, 251-268.
- Dugdale, S. J., Curry, R. A., St-Hilaire, A. & Andrews, S. N. 2018. Impact of future climate change on water temperature and thermal habitat for keystone fishes in the lower Saint John River, Canada. *Water Resources Management*, 32, 4853-4878.
- Dugdale, S. J., Hannah, D. M. & Malcolm, I. A. 2017. River temperature modelling: A review of process-based approaches and future directions. *Earth-Science Reviews*, 175, 97-113.
- Dugdale, S. J., Kelleher, C. A., Malcolm, I. A., Caldwell, S. & Hannah, D. M. 2019. Assessing the potential of drone-based thermal infrared imagery for quantifying river temperature heterogeneity. *Hydrological Processes*, 33, 1152-1163.
- Durmayaz, A. & Sogut, O. S. 2006. Influence of cooling water temperature on the efficiency of a pressurized-water reactor nuclear-power plant. *International Journal of Energy Research*, 30, 799-810.
- Eloranta, A. P., Finstad, A. G., Helland, I. P., Ugedal, O. & Power, M. 2018. Hydropower impacts on reservoir fish populations are modified by environmental variation. *Science of the total environment*, 618, 313-322.
- EPA, U. S. E. P. A. 2020. Temperature Water Quality Standards for the Columbia, Lower Columbia and Lower Snake Rivers.
- Ermida, S. L., Soares, P., Mantas, V., Götsche, F.-M. & Trigo, I. F. 2020. Google earth engine open-source code for land surface temperature estimation from the landsat series. *Remote Sensing*, 12, 1471.
- ESRI. 2016. *ArcGIS Model Builder [Archived]* [Online]. Available: <https://desktop.arcgis.com/en/arcmap/10.3/analyze/modelbuilder/what-is-modelbuilder.htm> [Accessed 10th August 2021].
- Färber, C., Lisniak, D., Saile, P., Kleber, S.-H., Ehl, M., Dietrich, S., Fader, M. & Demuth, S. Water quality at the global scale: GEMStat database and information system. EGU General Assembly Conference Abstracts, 2018. 15984.
- Foga, S., Scaramuzza, P. L., Guo, S., Zhu, Z., Dilley JR, R. D., Beckmann, T., Schmidt, G. L., Dwyer, J. L., Hughes, M. J. & Laue, B. 2017. Cloud detection algorithm comparison and validation for operational Landsat data products. *Remote sensing of environment*, 194, 379-390.
- Foley, A., Gallachóir, B. Ó., Hur, J., Baldick, R. & Mckeogh, E. 2010. A strategic review of electricity systems models. *Energy*, 35, 4522-4530.
- Fruchard, F. & Camenen, B. Reservoir sedimentation: different type of flushing-friendly flushing example of genissiat dam flushing. ICOLD International Symposium on Dams for a changing world, 2012. 6 p.
- Gamse, S., Zhou, W.-H., Tan, F., Yuen, K.-V. & Oberguggenberger, M. 2018. Hydrostatic-season-time model updating using Bayesian model class selection. *Reliability Engineering & System Safety*, 169, 40-50.
- Gardner, J. R., Yang, X., Topp, S. N., Ross, M. R. V., Altenau, E. H. & Pavelsky, T. M. 2021. The Color of Rivers. *Geophysical Research Letters*, 48, e2020GL088946.
- GEE, G. E. E. 2021a. *App Engine Example Apps* [Online]. Available: https://developers.google.com/earth-engine/guides/app_engine_examples [Accessed 17th August 2021].
- GEE, G. E. E. 2021b. *Earth Engine Data Catalogue* [Online]. Available: <https://developers.google.com/earth-engine/datasets> [Accessed 3rd March 2021].
- GEE, G. E. E. 2021c. *Google Earth Engine Code Editor* [Online]. Available: <https://code.earthengine.google.com/> [Accessed 1st January 2021].

- GEE, G. E. E. 2021d. *Guides - Statistics of an Image Region* [Online]. Available: https://developers.google.com/earth-engine/guides/reducers_reduce_region [Accessed 10th August 2021].
- GEE, G. E. E. 2021e. *Landsat Algorithms* [Online]. Available: <https://developers.google.com/earthengine/landsat> [Accessed April 10, 2021].
- Gorelick, N. Google earth engine. EGU General Assembly Conference Abstracts, 2013. 11997.
- Gorelick, N., Hancher, M., Dixon, M., Ilyushchenko, S., Thau, D. & Moore, R. 2017. Google Earth Engine: Planetary-scale geospatial analysis for everyone. *Remote sensing of Environment*, 202, 18-27.
- Granero-Belinchon, C., Michel, A., Achard, V. & Briottet, X. 2020. Spectral unmixing for thermal infrared multi-spectral airborne imagery over urban environments: day and night synergy. *Remote Sensing*, 12, 1871.
- Grumbine, R. E. & Xu, J. 2011. Mekong hydropower development. *Science*, 332, 178-179.
- Gu, J., Liu, M. & Tang, H. 2018. Analysis of the optical properties of typical surface emissivity based on the data of MODIS satellite telemetry. *Journal of Glaciology and Geocryology*, 04.
- Handcock, R., Gillespie, A., Cherkauer, K., Kay, J., Burges, S. & Kampf, S. 2006. Accuracy and uncertainty of thermal-infrared remote sensing of stream temperatures at multiple spatial scales. *Remote Sensing of Environment*, 100, 427-440.
- Handcock, R. N., Torgersen, C. E., Cherkauer, K. A., Gillespie, A. R., Tockner, K., Faux, R. N., Tan, J. & Carbonneau, P. 2012. Thermal infrared remote sensing of water temperature in riverine landscapes. *Fluvial remote sensing for science and management*, 1, 85-113.
- Hannah, D. M., Demuth, S., Van Lanen, H. A., Looser, U., Prudhomme, C., Rees, G., Stahl, K. & Tallaksen, L. M. 2011. Large-scale river flow archives: importance, current status and future needs. *Hydrological Processes*, 25, 1191-1200.
- Harris, C. R., Millman, K. J., Van Der Walt, S. J., Gommers, R., Virtanen, P., Cournapeau, D., Wieser, E., Taylor, J., Berg, S., Smith, N. J., Kern, R., Picus, M., Hoyer, S., Van Kerkwijk, M. H., Brett, M., Haldane, A., Del Río, J. F., Wiebe, M., Peterson, P., Gérard-Marchant, P., Sheppard, K., Reddy, T., Weckesser, W., Abbasi, H., Gohlke, C. & Oliphant, T. E. 2020. Array programming with NumPy. *Nature*, 585, 357-362.
- He, G., Zhang, Z., Jiao, W., Long, T., Peng, Y., Wang, G., Yin, R., Wang, W., Zhang, X., Liu, H., Cheng, B. & Xiang, B. 2018. Generation of ready to use (RTU) products over China based on Landsat series data. *Big Earth Data*, 2, 56-64.
- Heggenes, J., Alfredsen, K., Bustos, A. A., Huusko, A. & Stickler, M. 2018. Be cool: A review of hydro-physical changes and fish responses in winter in hydropower-regulated northern streams. *Environmental Biology of Fishes*, 101, 1-21.
- Hollstein, A., Segl, K., Guanter, L., Brell, M. & Enesco, M. 2016. Ready-to-use methods for the detection of clouds, cirrus, snow, shadow, water and clear sky pixels in Sentinel-2 MSI images. *Remote Sensing*, 8, 666.
- HRW, HR. Wallingford. 2021. *Dam Sat* [Online]. Available: <https://damsat.com/> [Accessed 30th July 2021].
- Hunter, J. D. 2007. Matplotlib: A 2D Graphics Environment. *Computing in Science & Engineering*, 9, 90-95.
- Ilyushchenko, S. 2021. *GIS - Stack Exchange: "Google Earth Engine - USGS Landsat 8 Level 2, Collection 2, Tier 1 metadata, should it differ from USGS guide?"* [Online]. Available: <https://gis.stackexchange.com/questions/402239/google-earth-engine-usgs-landsat-8-level-2-collection-2-tier-1-metadata-sho/402288#402288> [Accessed 23rd June 2021].
- Jensen, A. M., Mckee, M. & Chen, Y. Procedures for processing thermal images using low-cost microbolometer cameras for small unmanned aerial systems. 2014 IEEE Geoscience and Remote Sensing Symposium, 2014. IEEE, 2629-2632.
- Jensen, J. 2001. Managing fish, flood plains and food security in the Lower Mekong Basin. *Water Science and Technology*, 43, 157-164.

- Jiménez-Muñoz, J. C., Cristóbal, J., Sobrino, J. A., Sòria, G., Ninyerola, M. & Pons, X. 2008. Revision of the single-channel algorithm for land surface temperature retrieval from Landsat thermal-infrared data. *IEEE Transactions on geoscience and remote sensing*, 47, 339-349.
- Jiménez-Muñoz, J. C., Sobrino, J. A., Skoković, D., Mattar, C. & Cristóbal, J. 2014. Land surface temperature retrieval methods from Landsat-8 thermal infrared sensor data. *IEEE Geoscience and remote sensing letters*, 11, 1840-1843.
- Jiménez-Muñoz, J. C. & Sobrino, J. A. 2003. A generalized single-channel method for retrieving land surface temperature from remote sensing data. *Journal of geophysical research: atmospheres*, 108.
- Johann, F., Becker, D., Becker, M., Forsberg, R. & Kadir, M. 2019. The Direct Method in Strapdown Airborne Gravimetry—a Review. *zfv—Zeitschrift für Geodäsie, Geoinformation und Landmanagement*, 144, 323-333.
- Johnson, M. F. & Wilby, R. L. 2015. Seeing the landscape for the trees: metrics to guide riparian shade management in river catchments. *Water Resources Research*, 51, 3754-3769.
- Johnson, Z. C., Johnson, B. G., Briggs, M. A., Snyder, C. D., Hitt, N. P. & Devine, W. D. 2021. Heed the data gap: Guidelines for using incomplete datasets in annual stream temperature analyses. *Ecological Indicators*, 122, 107229.
- Kale, K. V., Solankar, M. M., Nalawade, D. B., Dhumal, R. K. & Gite, H. R. 2017. A research review on hyperspectral data processing and analysis algorithms. *Proceedings of the National Academy of Sciences, India Section A: Physical Sciences*, 87, 541-555.
- Kang, F., Li, J., Zhao, S. & Wang, Y. 2019. Structural health monitoring of concrete dams using long-term air temperature for thermal effect simulation. *Engineering Structures*, 180, 642-653.
- Kędra, M. 2020. Regional response to global warming: Water temperature trends in semi-natural mountain river systems. *Water*, 12, 283.
- Kędra, M. & Wiejaczka, Ł. 2018. Climatic and dam-induced impacts on river water temperature: Assessment and management implications. *Science of the Total Environment*, 626, 1474-1483.
- Kelly, J., Kljun, N., Olsson, P.-O., Mihai, L., Liljeblad, B., Weslien, P., Klemedtsson, L. & Eklundh, L. 2019. Challenges and best practices for deriving temperature data from an uncalibrated UAV thermal infrared camera. *Remote Sensing*, 11, 567.
- Kumar, L. & Mutanga, O. 2018. Google Earth Engine applications since inception: Usage, trends, and potential. *Remote Sensing*, 10, 1509.
- Lamaro, A. A., Mariñelarena, A., Torrusio, S. E. & Sala, S. E. 2013. Water surface temperature estimation from Landsat 7 ETM+ thermal infrared data using the generalized single-channel method: Case study of Embalse del Río Tercero (Córdoba, Argentina). *Advances in Space Research*, 51, 492-500.
- Lange, K., Meier, P., Trautwein, C., Schmid, M., Robinson, C. T., Weber, C. & Brodersen, J. 2018. Basin-scale effects of small hydropower on biodiversity dynamics. *Frontiers in Ecology and the Environment*, 16, 397-404.
- Ling, F., Foody, G. M., DU, H., Ban, X., Li, X., Zhang, Y. & Du, Y. 2017. Monitoring thermal pollution in rivers downstream of dams with Landsat ETM+ thermal infrared images. *Remote Sensing*, 9, 1175.
- Liu, S., Xie, Z., Liu, B., Wang, Y., Gao, J., Zeng, Y., Xie, J., Xie, Z., Jia, B. & Qin, P. 2020. Global river water warming due to climate change and anthropogenic heat emission. *Global and Planetary Change*, 193, 103289.
- Liu, Z., Zhang, Z., Zhuo, R. & Wang, X. 2019. Optimal operation of independent regional power grid with multiple wind-solar-hydro-battery power. *Applied energy*, 235, 1541-1550.
- Loyola-Gonzalez, O. 2019. Black-box vs. white-box: Understanding their advantages and weaknesses from a practical point of view. *IEEE Access*, 7, 154096-154113.
- Mäkinen, T., Leinonen, A. & Ovaskainen, M. Modelling and benefits of combined operation of hydropower unit and battery energy storage system on grid primary frequency control.

- 2020 IEEE International Conference on Environment and Electrical Engineering and 2020 IEEE Industrial and Commercial Power Systems Europe (EEEIC/I&CPS Europe), 2020. IEEE, 1-6.
- Markham, B. L. & Barker, J. L. 1985. Spectral characterization of the Landsat Thematic Mapper sensors. *International Journal of Remote Sensing*, 6, 697-716.
- Martí-Cardona, B., Prats, J. & Niclòs, R. 2019. Enhancing the retrieval of stream surface temperature from Landsat data. *Remote Sensing of Environment*, 224, 182-191.
- Masek, J. G., Wulder, M. A., Markham, B., Mccorkel, J., Crawford, C. J., Storey, J. & Jenstrom, D. T. 2020. Landsat 9: Empowering open science and applications through continuity. *Remote Sensing of Environment*, 248, 111968.
- Mckinney, W. Data structures for statistical computing in python. Proceedings of the 9th Python in Science Conference, 2010. Austin, TX, 51-56.
- Melchiorre, A., Boschetti, L. & Roy, D. P. 2020. Global Evaluation of the Suitability of MODIS-Terra Detected Cloud Cover as a Proxy for Landsat 7 Cloud Conditions. *Remote Sensing*, 12, 202.
- Meng, X. & Cheng, J. 2018. Evaluating eight global reanalysis products for atmospheric correction of thermal infrared sensor—Application to Landsat 8 TIRS10 Data. *Remote Sensing*, 10, 474.
- Meng, Y., Liu, J., Leduc, S., Mesfun, S., Kraxner, F., Mao, G., Qi, W. & Wang, Z. 2020. Hydropower production benefits more from 1.5 C than 2 C climate scenario. *Water Resources Research*, 56, e2019WR025519.
- Mo, F., Li, H., Jing, Q., Zhang, X., Cao, B. & Liu, Q. Research on high resolution thermal infrared satellite technology and applications. IGARSS 2018-2018 IEEE International Geoscience and Remote Sensing Symposium, 2018. IEEE, 5674-5677.
- Mohseni, O., Stefan, H. G. & Erickson, T. R. 1998. A nonlinear regression model for weekly stream temperatures. *Water Resources Research*, 34, 2685-2692.
- Montanaro, M., Gerace, A., Lunsford, A. & Reuter, D. 2014. Stray light artifacts in imagery from the Landsat 8 Thermal Infrared Sensor. *Remote Sensing*, 6, 10435-10456.
- Montanaro, M., Gerace, A. & Rohrbach, S. 2015. Toward an operational stray light correction for the Landsat 8 Thermal Infrared Sensor. *Applied Optics*, 54, 3963-3978.
- Montero, D. 2021. Eemont: A Python package that extends Google Earth Engine. *Journal of Open Source Software* 6, 3168.
- Moore, D., Dore, J. & Gyawali, D. 2010. The World Commission on Dams+ 10: Revisiting the large dam controversy. *Water Alternatives*, 3, 3.
- Mulatu, A., Gerlagh, R., Rigby, D. & Wossink, A. 2010. Environmental regulation and industry location in Europe. *Environmental and Resource Economics*, 45, 459-479.
- Munk, M. & Turk, M. J. 2020. widgyts: Custom Jupyter Widgets for Interactive Data Exploration with yt. *Journal of Open Source Software*, 5, 1774.
- Mutanga, O. & Kumar, L. 2019. Google earth engine applications. Multidisciplinary Digital Publishing Institute.
- Navarro, J. A. First Experiences with Google Earth Engine. GISTAM, 2017. 250-255.
- Olden, J. D. & Naiman, R. J. 2010. Incorporating thermal regimes into environmental flows assessments: modifying dam operations to restore freshwater ecosystem integrity. *Freshwater Biology*, 55, 86-107.
- Ouellet-Proulx, S., Chimi Chiadjeu, O., Boucher, M.-A. & St-Hilaire, A. 2017. Assimilation of water temperature and discharge data for ensemble water temperature forecasting. *Journal of Hydrology*, 554, 342-359.
- Ouellet, V., St-Hilaire, A., Dugdale, S. J., Hannah, D. M., Krause, S. & Proulx-Ouellet, S. 2020. River temperature research and practice: Recent challenges and emerging opportunities for managing thermal habitat conditions in stream ecosystems. *Science of The Total Environment*, 139679.

- Pavelsky, T. M., Durand, M. T., Andreadis, K. M., Beighley, R. E., Paiva, R. C., Allen, G. H. & Miller, Z. F. 2014. Assessing the potential global extent of SWOT river discharge observations. *Journal of Hydrology*, 519, 1516-1525.
- Perkel, J. M. 2018. Data visualization tools drive interactivity and reproducibility in online publishing. *Nature*, 554, 133-134.
- Piccolroaz, S., Calamita, E., Majone, B., Gallice, A., Siviglia, A. & Toffolon, M. 2016. Prediction of river water temperature: a comparison between a new family of hybrid models and statistical approaches. *Hydrological Processes*, 30, 3901-3917.
- Piégay, H., Arnaud, F., Belletti, B., Bertrand, M., Bizzi, S., Carbonneau, P., Dufour, S., Liébault, F., Ruiz-Villanueva, V. & Slater, L. 2020. Remotely sensed rivers in the Anthropocene: State of the art and prospects. *Earth Surface Processes and Landforms*, 45, 157-188.
- Pilla, R. M., Mette, E. M., Williamson, C. E., Adamovich, B. V., Adrian, R., Anneville, O., Balseiro, E., Ban, S., Chandra, S. & Colom-Montero, W. 2021. Global data set of long-term summertime vertical temperature profiles in 153 lakes. *Scientific data*, 8, 1-12.
- Piotrowski, A. P., Osuch, M. & Napiorkowski, J. J. 2021. Influence of the choice of stream temperature model on the projections of water temperature in rivers. *Journal of Hydrology*, 126629.
- Planck, M. 1914. *The theory of heat radiation*, Courier Corporation.
- Qin, Z., Karnieli, A. & Berliner, P. 2001. A mono-window algorithm for retrieving land surface temperature from Landsat TM data and its application to the Israel-Egypt border region. *International journal of remote sensing*, 22, 3719-3746.
- Rheinheimer, D. E., Null, S. E. & Lund, J. R. 2015. Optimizing selective withdrawal from reservoirs to manage downstream temperatures with climate warming. *Journal of Water Resources Planning and Management*, 141, 04014063.
- Roy, S. 2020. *Community Datasets & Data Commons in Google Earth Engine* [Online]. Available: <https://medium.com/geospatial-processing-at-scale/community-datasets-data-commons-in-google-earth-engine-8585d8baef1f> [Accessed 5th July 2021].
- Rozenstein, O., Qin, Z., Derimian, Y. & Karnieli, A. 2014. Derivation of land surface temperature for Landsat-8 TIRS using a split window algorithm. *Sensors*, 14, 5768-5780.
- Schluessel, P., Emery, W. J., Grassl, H. & Mammen, T. 1990. On the bulk-skin temperature difference and its impact on satellite remote sensing of sea surface temperature. *Journal of Geophysical Research: Oceans*, 95, 13341-13356.
- Schmid, N., Haelg, L., Sewerin, S., Schmidt, T. S. & Simmen, I. 2020. Governing complex societal problems: The impact of private on public regulation through technological change. *Regulation & Governance*.
- Sherman, B. 2000. *Scoping options for mitigating cold water discharges from dams*, CSIRO Land and Water Canberra.
- Shi, H., Chen, J., Liu, S. & Sivakumar, B. 2019. The role of large dams in promoting economic development under the pressure of population growth. *Sustainability*, 11, 2965.
- Shi, X., Sun, J. & Xiao, Z. 2021. Investigation on River Thermal Regime under Dam Influence by Integrating Remote Sensing and Water Temperature Model. *Water*, 13, 133.
- Shree, S., Kumar, M. & Singh, A. 2021. Exploring spatial and temporal trends of diurnal temperature range in the region of the Subarnarekha river basin India. *Spatial Information Research*, 29, 149-162.
- Skalak, K. J., Benthem, A. J., Schenk, E. R., Hupp, C. R., Galloway, J. M., Nustad, R. A. & Wiche, G. J. 2013. Large dams and alluvial rivers in the Anthropocene: The impacts of the Garrison and Oahe Dams on the Upper Missouri River. *Anthropocene*, 2, 51-64.
- Sobrino, J. A., Jiménez-Muñoz, J. C., Sòria, G., Romaguera, M., Guanter, L., Moreno, J., Plaza, A. & Martínez, P. 2008. Land surface emissivity retrieval from different VNIR and TIR sensors. *IEEE transactions on geoscience and remote sensing*, 46, 316-327.

- Sowder, C. & Steel, E. A. 2012. A note on the collection and cleaning of water temperature data. *Water*, 4, 597-606.
- SPYDER. 2021. Available: <https://github.com/spyder-ide/spyder/wiki/SEP-6:-Spyder-API> [Accessed 3rd January 2020].
- Srinivasan, R. & Sorial, G. A. 2011. Treatment of taste and odor causing compounds 2-methyl isoborneol and geosmin in drinking water: A critical review. *Journal of Environmental Sciences*, 23, 1-13.
- Stoll, B., Andrade, J., Cohen, S., Brinkman, G. & Brancucci Martinez-Anido, C. 2017. Hydropower modeling challenges. National Renewable Energy Lab.(NREL), Golden, CO (United States).
- Tabari, M. M. R., Azadani, M. N. & Kamgar, R. 2020. Development of operation multi-objective model of dam reservoir under conditions of temperature variation and loading using NSGA-II and DANN models: a case study of Karaj/Amir Kabir dam. *Soft Computing*, 24, 12469-12499.
- Talke, S. A., Horner-Devine, A. R., Chickadel, C. C. & Jessup, A. T. 2013. Turbulent kinetic energy and coherent structures in a tidal river. *Journal of Geophysical Research: Oceans*, 118, 6965-6981.
- Tamiminia, H., Salehi, B., Mahdianpari, M., Quackenbush, L., Adeli, S. & Brisco, B. 2020. Google Earth Engine for geo-big data applications: A meta-analysis and systematic review. *ISPRS Journal of Photogrammetry and Remote Sensing*, 164, 152-170.
- Tatin, M., Briffaut, M., Dufour, F., Simon, A. & Fabre, J.-P. 2018. Statistical modelling of thermal displacements for concrete dams: Influence of water temperature profile and dam thickness profile. *Engineering Structures*, 165, 63-75.
- Tavares, M. H., Cunha, A. H. F., Motta-Marques, D., Ruhoff, A. L., Fragoso JR, C. R., Munar, A. M. & Bonnet, M.-P. 2020. Derivation of consistent, continuous daily river temperature data series by combining remote sensing and water temperature models. *Remote Sensing of Environment*, 241, 111721.
- Toffolon, M. & Piccolroaz, S. 2015. A hybrid model for river water temperature as a function of air temperature and discharge. *Environmental Research Letters*, 10, 114011.
- Torgersen, C. E., Faux, R. N., Mcintosh, B. A., Poage, N. J. & Norton, D. J. 2001. Airborne thermal remote sensing for water temperature assessment in rivers and streams. *Remote Sensing of Environment*, 76, 386-398.
- USGS 2020. Landsat 8 Collection 2 (C2) Level 2 Science Product (L2SP) Guide.
- USGS, U. S. G. S. 2018. *Landsat Multispectral Scanner (MSS) Level 1 (L1) Data Format Control Book (DFCB)* [Online]. Available: https://prd-wret.s3.us-west-2.amazonaws.com/assets/palladium/production/atoms/files/LSDS-286_LandsatMSS-Level1_DFCB-v11.pdf [Accessed 29th June 2021].
- USGS, U. S. G. S. 2019a. *Landsat 7 (L7) Data Users Handbook* [Online]. Available: https://prd-wret.s3.us-west-2.amazonaws.com/assets/palladium/production/atoms/files/LSDS-1927_L7_Data_Users_Handbook-v2.pdf [Accessed 6th July 2021].
- USGS, U. S. G. S. 2019b. *Landsat 8 (L8) Data Users Handbook: Collection 1* [Online]. Available: https://prd-wret.s3.us-west-2.amazonaws.com/assets/palladium/production/atoms/files/LSDS-1574_L8_Data_Users_Handbook-v5.0.pdf [Accessed 5th January 2021].
- USGS, U. S. G. S. 2021a. Earth Explorer data download.
- USGS, U. S. G. S. 2021b. *Grand Canyon Monitoring and Research Center - Grand Canyon Stations* [Online]. Available: https://www.gcmrc.gov/discharge_qw_sediment/stations/GCDAMP/ [Accessed 29th June 2021].
- USGS, U. S. G. S. 2021c. *MODIS Overview* [Online]. Available: <https://lpdaac.usgs.gov/data/get-started-data/collection-overview/missions/modis-overview/#modis-tools-and-services> [Accessed 13th August 2021].
- VALMAN, S. 2021a. *RiverTemperatureAPP* [Online]. Heroku APPS. Available: <https://calm-temple-96811.herokuapp.com/> [Accessed 16th August 2021].

- VALMAN, S. 2021b. *SatTemp Github/PIP Python Package* [Online]. Available: <https://github.com/SamValman/rtemp> [Accessed 3rd August 2021].
- Van Vliet, M. T., Franssen, W. H., Yearsley, J. R., Ludwig, F., Haddeland, I., Lettenmaier, D. P. & Kabat, P. 2013. Global river discharge and water temperature under climate change. *Global Environmental Change*, 23, 450-464.
- Virtanen, P., Gommers, R., Oliphant, T. E., Haberland, M., Reddy, T., Cournapeau, D., Burovski, E., Peterson, P., Weckesser, W. & Bright, J. 2020. SciPy 1.0: fundamental algorithms for scientific computing in Python. *Nature methods*, 17, 261-272.
- Voichick, N. & Wright, S. A. Water-Temperature Data for the Colorado River and Tributaries Between Glen Canyon Dam and Spencer Canyon, Northern Arizona, 1988-2005. 2007.
- Wang, C., Jia, M., Chen, N. & Wang, W. 2018. Long-term surface water dynamics analysis based on Landsat imagery and the Google Earth Engine platform: A case study in the middle Yangtze River Basin. *Remote Sensing*, 10, 1635.
- Wang, L., Diao, C., Xian, G., Yin, D., Lu, Y., Zou, S. & Erickson, T. A. 2020a. A summary of the special issue on remote sensing of land change science with Google earth engine. Elsevier.
- Wang, L. T. & De Liberty, T. L. Landsat Atmospheric Correction: The Good, the Bad, and the Ugly. 2005 ESRI International User Conference Proc, 2005.
- Wang, M., Zhang, Z., Hu, T. & Liu, X. 2019a. A practical single-channel algorithm for land surface temperature retrieval: application to Landsat series data. *Journal of Geophysical Research: Atmospheres*, 124, 299-316.
- Wang, M., Zhang, Z., Hu, T., Wang, G., He, G., Zhang, Z., Li, H., Wu, Z. & Liu, X. 2020b. An Efficient Framework for Producing Landsat-Based Land Surface Temperature Data Using Google Earth Engine. *IEEE Journal of Selected Topics in Applied Earth Observations and Remote Sensing*, 13, 4689-4701.
- Wang, S., Shen, W., Tang, W., Wang, Y., Duffield, C. F. & Hui, F. K. P. 2019b. Understanding the social network of stakeholders in hydropower project development: An owners' view. *Renewable Energy*, 132, 326-334.
- Wawrzyniak, V., Piégay, H. & Poirol, A. 2012. Longitudinal and temporal thermal patterns of the French Rhône River using Landsat ETM+ thermal infrared images. *Aquatic sciences*, 74, 405-414.
- Weber, M., Rinke, K., Hipsey, M. & Boehrer, B. 2017. Optimizing withdrawal from drinking water reservoirs to reduce downstream temperature pollution and reservoir hypoxia. *Journal of environmental management*, 197, 96-105.
- Wilby, R. L., Orr, H., Watts, G., Battarbee, R. W., Berry, P. M., Chadd, R., Dugdale, S. J., Dunbar, M. J., Elliott, J. A., Extence, C., Hannah, D. M., Holmes, N., Johnson, A. C., Knights, B., Milner, N. J., Ormerod, S. J., Solomon, D., Timlett, R., Whitehead, P. J. & Wood, P. J. 2010. Evidence needed to manage freshwater ecosystems in a changing climate: Turning adaptation principles into practice. *Science of The Total Environment*, 408, 4150-4164.
- Wright, S. A., Anderson, C. R. & Voichick, N. 2009. A simplified water temperature model for the Colorado River below Glen Canyon Dam. *River Research and Applications*, 25, 675-686.
- Wu, H., Chen, J., Xu, J., Zeng, G., Sang, L., Liu, Q., Yin, Z., Dai, J., Yin, D., Liang, J. & Ye, S. 2019. Effects of dam construction on biodiversity: A review. *Journal of Cleaner Production*, 221, 480-489.
- Wu, Q. 2020. geemap: A Python package for interactive mapping with Google Earth Engine. *Journal of Open Source Software*, 5, 2305.
- Xie, C. Research and application of key technologies for dam safety monitoring based on LoRa. IOP Conference Series: Earth and Environmental Science, 2021. IOP Publishing, 012131.
- Xiong, Y. J., Yin, J., Zhao, S. H., Qiu, G. Y. & Liu, Z. 2020. How the three Gorges Dam affects the hydrological cycle in the mid-lower Yangtze River: a perspective based on decadal water temperature changes. *Environmental Research Letters*, 15, 014002.
- Yadav, N. A., Ohri, A. & Das, N. 2020. Analysis of Thermal Pattern Variation for River Ganges with Satellite Imagery.

- Yang, X., Pavelsky, T. M. & Allen, G. H. 2020. The past and future of global river ice. *Nature*, 577, 69-73.
- Yang, X., Pavelsky, T. M., Allen, G. H. & Donchyts, G. 2019. RivWidthCloud: An automated Google Earth Engine algorithm for river width extraction from remotely sensed imagery. *IEEE Geoscience and Remote Sensing Letters*, 17, 217-221.
- Young, N. E., Anderson, R. S., Chignell, S. M., Vorster, A. G., Lawrence, R. & Evangelista, P. H. 2017. A survival guide to Landsat preprocessing. *Ecology*, 98, 920-932.
- Zhao, J., Li, H., Cai, X., Chen, F., Wang, L. & Yu, D. 2020. Long-term (2002–2017) impacts of Danjiangkou dam on thermal regimes of downstream Han River (China) using Landsat thermal infrared imagery. *Journal of Hydrology*, 589, 125135.
- Zhu, Z. & Woodcock, C. E. 2012. Object-based cloud and cloud shadow detection in Landsat imagery. *Remote sensing of environment*, 118, 83-94.
- Zhu, Z., Wulder, M. A., Roy, D. P., Woodcock, C. E., Hansen, M. C., Radeloff, V. C., Healey, S. P., Schaaf, C., Hostert, P. & Strobl, P. 2019. Benefits of the free and open Landsat data policy. *Remote Sensing of Environment*, 224, 382-385.

Appendix A

N	Date	Time	Row	Path	Cloud Cover (%)
Colorado River logger: 404200	2013-04-22	18:11:10	35	38	0
	2013-05-24	18:11:26	35	38	7
	2013-06-09	18:11:24	35	38	0
	2013-06-25	18:11:20	35	38	0
	2013-07-27	18:11:22	35	38	65.3
	2013-08-12	18:11:24	35	38	6.5
	2013-08-28	18:11:26	35	38	11.3
	2013-09-13	18:11:22	35	38	3.7
	2013-09-29	18:11:16	35	38	0.1
	2013-10-15	18:11:15	35	38	2.7
	2013-10-31	18:11:07	35	38	0.3
	2013-12-02	18:11:01	35	38	0.1
	2014-01-03	18:10:45	35	38	0.2
	2014-01-19	18:10:32	35	38	6.8
	2014-02-04	18:10:24	35	38	15.6
	2014-02-20	18:10:11	35	38	0.3
	2014-03-08	18:09:57	35	38	0.4
	2014-04-09	18:09:29	35	38	46.1
	2014-04-25	18:09:13	35	38	24.2
	2014-05-27	18:08:56	35	38	1.3
	2014-06-12	18:09:05	35	38	0.5
	2014-06-28	18:09:07	35	38	0
	2014-07-30	18:09:20	35	38	12.4
	2014-08-15	18:09:27	35	38	7.4
	2014-08-31	18:09:29	35	38	0
	2014-09-16	18:09:31	35	38	1.8
	2014-10-02	18:09:34	35	38	0
	2014-10-18	18:09:37	35	38	55.7
	2014-11-03	18:09:36	35	38	9.5
	2014-12-05	18:09:33	35	38	60.6
	2014-12-21	18:09:31	35	38	42.8
	2015-01-06	18:09:26	35	38	2.1
	2015-01-22	18:09:20	35	38	0.4
	2015-03-27	18:08:53	35	38	0.4
	2015-04-12	18:08:46	35	38	0.1
	2015-04-28	18:08:40	35	38	7.4
	2015-05-30	18:08:29	35	38	4.3
	2015-06-15	18:08:41	35	38	7.8
	2015-07-01	18:08:47	35	38	0
	2015-07-17	18:08:57	35	38	1.9
2015-08-02	18:09:00	35	38	23.5	
2015-08-18	18:09:08	35	38	0.3	
2015-09-03	18:09:12	35	38	1.5	
2015-09-19	18:09:21	35	38	0	
2015-11-06	18:09:30	35	38	0.6	

Colorado River logger: 404200

2015-11-22	18:09:32	35	38	0.2
2015-12-08	18:09:30	35	38	1.1
2015-12-24	18:09:32	35	38	44.3
2016-01-09	18:09:27	35	38	15.1
2016-01-25	18:09:28	35	38	0.2
2016-02-26	18:09:17	35	38	0.4
2016-03-13	18:09:14	35	38	13.4
2016-03-29	18:09:04	35	38	54.9
2016-06-01	18:09:03	35	38	0.4
2016-06-17	18:09:06	35	38	0
2016-07-19	18:09:22	35	38	32
2016-08-20	18:09:30	35	38	3.5
2016-09-05	18:09:36	35	38	0.1
2016-10-07	18:09:41	35	38	0
2016-10-23	18:09:44	35	38	38.3
2016-11-08	18:09:43	35	38	0
2016-11-24	18:09:44	35	38	0.1
2016-12-10	18:09:41	35	38	9.6
2016-12-26	18:09:37	35	38	4.4
2017-01-11	18:09:34	35	38	36.8
2017-01-27	18:09:28	35	38	0.2
2017-02-28	18:09:15	35	38	36.3
2017-03-16	18:09:06	35	38	0.3
2017-04-01	18:08:58	35	38	28.2
2017-04-17	18:08:49	35	38	34.5
2017-05-03	18:08:40	35	38	0
2017-05-19	18:08:52	35	38	0.1
2017-06-04	18:09:01	35	38	2.8
2017-06-20	18:09:07	35	38	3
2017-07-06	18:09:11	35	38	8.4
2017-07-22	18:09:17	35	38	3.7
2017-08-07	18:09:24	35	38	14
2017-08-23	18:09:28	35	38	15.8
2017-09-24	18:09:35	35	38	0.1
2017-10-10	18:09:40	35	38	0
2017-10-26	18:09:41	35	38	1.5
2017-11-11	18:09:39	35	38	1.4
2017-12-13	18:09:33	35	38	2.4
2018-01-14	18:09:27	35	38	0
2018-02-15	18:09:12	35	38	0.3
2018-03-03	18:09:04	35	38	65.3
2018-03-19	18:08:55	35	38	17.2
2018-06-07	18:08:11	35	38	2.9
2018-06-23	18:08:22	35	38	0
2018-07-25	18:08:37	35	38	0
2018-08-10	18:08:47	35	38	8.7
2018-09-11	18:09:04	35	38	0.2
2018-09-27	18:09:11	35	38	0
2018-11-14	18:09:6	35	38	0
2018-12-16	18:09:20	35	38	17.6
2019-01-01	18:09:25	35	38	0.2
2019-03-22	18:09:31	35	38	50.4
2019-04-07	18:09:35	35	38	18.3
2019-04-23	18:09:40	35	38	3.2
2019-05-25	18:09:44	35	38	1.7

Saint John River

2019-06-10	18:09:47	35	38	0.3
2019-06-26	18:09:47	35	38	5.3
2019-07-12	18:09:43	35	38	72.4
2019-07-28	18:09:42	35	38	17.2
2019-08-13	18:09:36	35	38	0
2019-08-29	18:09:32	35	38	0
2019-09-14	18:09:27	35	38	0
2019-09-30	18:09:24	35	38	0
2019-10-16	18:09:10	35	38	0.4
2019-11-01	18:09:01	35	38	0
2019-11-17	18:08:54	35	38	0
2019-12-03	18:08:47	35	38	53
2020-01-04	18:08:51	35	38	26.5
2020-01-20	18:09:01	35	38	95.7
2020-02-05	18:08:54	35	38	28.7
2020-02-21	18:08:47	35	38	1.5
2020-03-24	18:08:51	35	38	3.7
2020-04-09	18:09:01	35	38	33.4
2020-04-25	18:09:09	35	38	0.1
2020-05-11	18:09:15	35	38	0.6
2020-05-27	18:09:20	35	38	0.2
2020-06-12	18:09:24	35	38	0
2020-06-28	18:09:32	35	38	7.8
2020-07-14	18:09:38	35	38	0.1
2020-07-30	18:09:42	35	38	0.1
2020-08-15	18:09:43	35	38	0.1
2020-08-31	18:09:42	35	38	2.4
2020-09-16	18:09:44	35	38	0.4
2020-10-02	18:09:25	35	38	0
2020-10-18	18:09:17	35	38	0
2020-11-19	18:09:14	35	38	0.2
2020-12-05	18:08:57	35	38	0.1
2021-02-23	18:09:02	35	38	0.4
2021-07-01	18:09:31	35	38	18.8
2014-07-26	15:13:27	28	10	21.4
2014-07-26	15:13:36	28	10	6.2
2014-08-27	15:13:38	28	10	49.6
2014-09-12	15:13:42	28	10	3.5
2014-09-28	15:13:41	28	10	0
2014-10-14	15:13:47	28	10	23.8
2014-10-30	15:13:43	28	10	29
2015-06-27	15:12:54	28	10	10.2
2015-07-13	15:13:05	28	10	6.8
2015-07-29	15:13:10	28	10	8.5
2015-08-14	15:13:15	28	10	19.9
2015-09-15	15:13:29	28	10	18.4
2015-12-04	15:13:41	28	10	20.8
2015-07-13	15:13:05	28	10	6.8
2015-07-29	15:13:10	28	10	8.5
2014-08-11	15:13:36	28	10	6.2
2015-08-30	15:13:21	28	10	50.8
2014-11-15	15:13:46	28	10	57.4
2015-09-06	15:19:35	28	11	0
2015-10-08	15:19:45	29	11	6.8

River Ganges

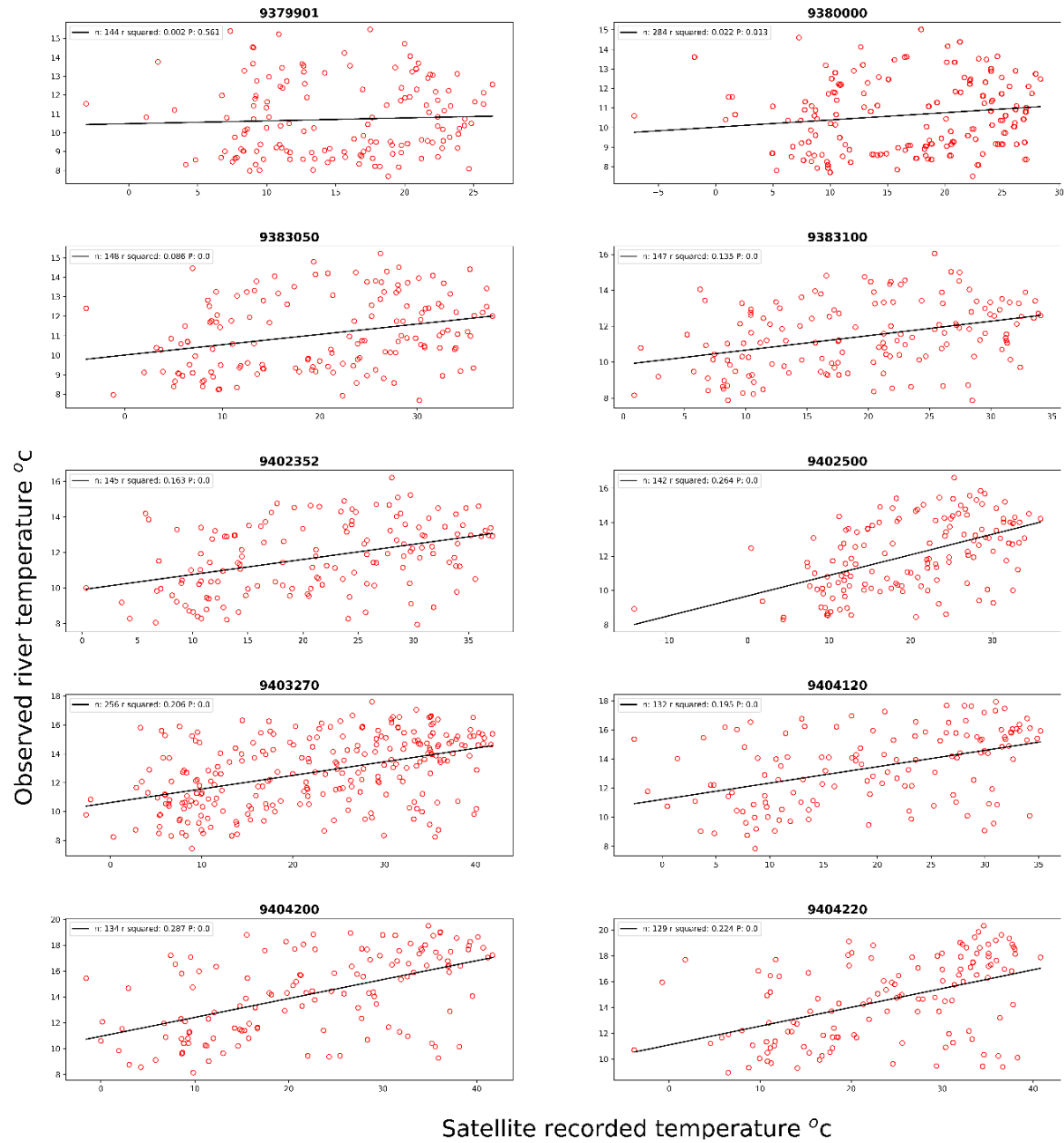
2015-02-16	04:54:44	42	142	0
2017-02-21	04:54:50	42	142	0.6
2018-02-24	04:54:40	42	142	13.1

Appendix B

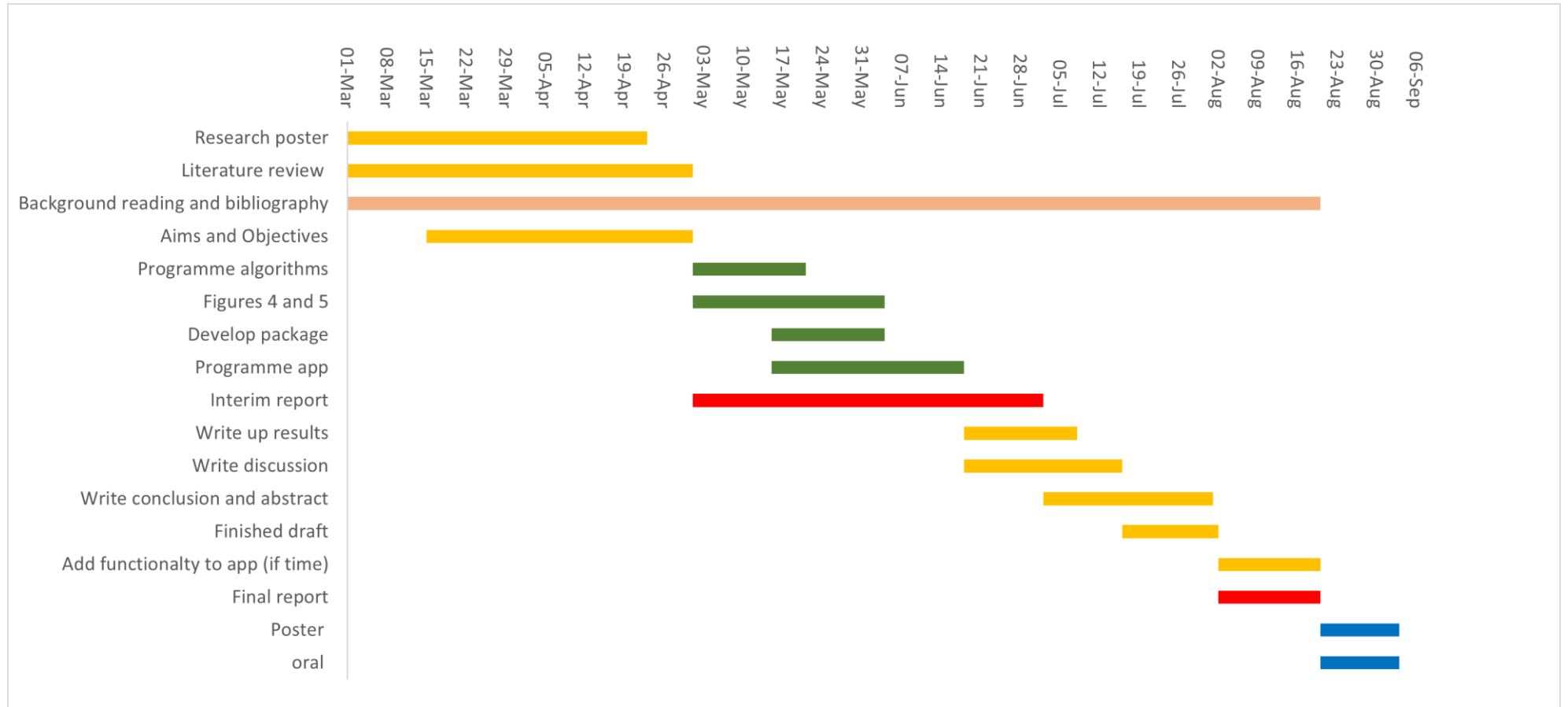
Validation results from Glen Canyon, the lack of strong correlations are discussed in section 6.2.2. As the highest correlation, only site 9404200 was chosen to represent these results within the text.

Site	9379901	9380000	9383050	9383100	9402352	9402500	9403270	9404120	9404200	9404220
N	144	284	148	147	145	142	256	132	134	129
images										
R²	0.002	0.022	0.086	0.135	0.163	0.264	0.206	0.195	0.287	0.224
P	0.561	0.013*	<0.001*	<0.001*	<0.001*	<0.001*	<0.001*	<0.001*	<0.001*	<0.001*
RMSE	7.88	9.32	13.5	11.3	12.8	11.2	14.4	11.1	13.1	13.1
Bias	4.56	5.87	9.19	7.91	9.53	7.85	9.73	6.27	8.32	9.31

* Significant at the 0.05 alpha level



Project Management Plan



Data Management Plan

Research title, aims and objectives

Title

An assessment of the potential for cloud computing and satellite thermal infrared sensing to produce meaningful river temperature insights for hydropower operations

Aim

Assess the viability of using Google Earth Engine for the extraction of river temperature outputs for assisting dam and industrial operating procedures globally.

Objectives

Objective 1: Verify the ability of GEE as a tool for calculating river surface temperature from satellite TIR inputs to produce an interactive tool for extracting river temperature.

Objective 2: Validate the accuracy of the results against different river types to infer the transferability of the method

Objective 3: Compare different atmospheric correction methods to assess which produces the most accurate results

Methodology and data types produced

River temperature measurement values will be produced from freely available Landsat 8 images. With the exception of 6 tiff files used for longitudinal diagrams. This data will not be stored, instead the Python Jupyter Notebook scripts will be stored to recompute the results using Google Earth Engine Servers.

Processing requires multiple Jupyter Notebook files written with Python 3 for the majority of the project. The Python package will be written in the Spyder API to facilitate the possibility of uploading it to PiP to be freely installed by other users. A Heroku app will also be produced which is powered through a GitHub repository.

Landsat scenes used can be found in Appendix A of this document.

Metadata content and format

Metadata was based on the EU INSPIRE metadata standards.

All files will be saved with the following metadata and be backed up by a version control system (GitHub) to establish order and timing of changes:

- Filename
- Item type (e.g. tif)
- Size (mb or GEE pixels)
- Description of script task/aim
- dependencies (requirements.txt file)
- Creation timestamp
- Last edit
- Location = (long lat or geometry)
- Owner and copyright or access agreements

Project structure and storage

All data will be saved on the University OneDrive which is backed up by the central University IT System. This will have a secondary GitHub back up procedure to a repository to provide better versioning control. This push request will be carried out at the end of every day.

Code and validation data repository: https://github.com/SamValman/MRes_2021

SatTemp package repository: <https://github.com/SamValman/rtemp>

Access will have to be requested from these weblinks and the primary author will confirm access.

All filenames will start with the date “YYYY_MM_DD_”

Folders in a package will be structured hierarchically starting with “00”

The site and method will be used to indicate the objective of these folders, whilst the task will be used to indicate the objective of scripts.

Data sharing at project completion

During the project, including the duration of the PhD (until October 2024) data will be shared between the principal researcher and supervisors, along with collaborators and CDT directors upon request.

Dissemination projects will be shared through apps and GitHub packages which are currently set to private until project completion. Validation data (.csv files) will be placed in a repository so results can be confirmed upon completion of the project.

Data selection and long-term preservation

Python scripts with the dependencies made clear in the metadata will enable the reproducibility of the results using opensource software which can later be rolled back to versions used during the project if required.

Validation data and data used for figures published in these projects will be placed in open access archives to enable preservation and transparency.

Responsibilities of the Data Management Plan

The first and final responsibility of implementing the data management plan is the lead researcher in this project (Sam Valman). Access to the Nottingham University OneDrive or personal Github repository will be required to enact this plan. Supervisors will be given contributor rights to this Github account to enable their contribution if required.

If the project changes from what is presented here in this MRes then this data management plan and the data storage/data sharing options will be re-evaluated accordingly.